AN INVESTIGATION OF SILICON CRYSTAL DEFECTS CAUSED BY BORON DOPING

Bachelor's Thesis

zur Erlangung des akademischen Grades
Bachelor of Science
der Studienrichtung Technische Physik

Andreas Jörg Schriefl

durchgeführt bei
Infineon Technologies Austria AG
in kooperation mit dem
Institut für Festkörperphysik
an der

Technischen Universität Graz

Betreuer:
O.Univ.-Prof. Dr.Phil. Hartmut Kahlert
Mitbetreut durch:
Dr.Techn. Sokratis Sgouridis

März 2008

Meinen Eltern, meiner Schwester und Monica gewidmet.

Abstract

In silicon processing technology, one of the primary objectives is to achieve a controlled impurity doping in the silicon substrate to produce n-type or p-type areas. A fast and critical doping process is ion implantation through an implantor, followed by a diffusion process through oven processes. The principal advantages of this method are the accurate adjustability of the implantation dose, the avoidance of high process temperatures, the structuring of the implanted areas using standard masking methods, and the accurate and reproducible influence upon the shape and depth of the doping profile. A problematic disadvantage of ion implantation is the occurrence of crystal damage in the silicon substrate caused by ion bombardement. In semiconductor technology, those crystal defects have a negative influence upon the electrical activity in the depletion zone as well as on the diffusion properties of the doped atoms.

Throughout this paper, a broad survey of the influence of high boron implantation and the subsequent diffusion process upon crystal defect generation will be presented. Special attention was paid to the way in which defect formation is influenced by the following parameters: implantation dose, implantation energy, beam current, and different diffusion processes. Software simulations were conducted during which the values of those parameters varied to differing degrees. Based on these results, as well as on discussions with field experts, a new set of experiments has been defined. The results of the experiments have been analysed and compared with literature values when available. Additionally, the influence upon defect formation of a silicon backside getter layer and the influence of a higher oxygen concentration in the substrate material have been scrutinized. Throughout the writing of this paper, a known detection method was modified so as to detect the defect distribution on the entire wafer of this series in a short period of time.

To initiate the presentation of this study, the basics of semiconductor technology and the methods for crystal defect detection and analysis used during the writing of this paper will be briefly described. To ensure the reader's complete understanding of the production process up to the point when the defects begin to occur, an explanatory diagram has been included. The final chapter examines the theoretical background of ion implantation. Predictions of the theories about defect formation and range distribution of implanted ions have been compared with the results of the simulations and experiments conducted in this study.

In der Halbleiterverfahrenstechnik ist ein wichtiges Ziel die kontrollierte Dotierung mit Fremdatomen zur Herstellung von Verarmungszonen im Silizium Grundmaterial. Ein schnelles und sehr wichtiges Dotierverfahren ist die Ionenimplantation durch einen Implantor mit anschließender Diffusion durch Ofenprozesse. Die entscheidenden Vorteile dieser Methode liegen in der genauen Kontrollierbarkeit der Implantationsdosis, der Vermeidung hoher Prozesstemperaturen, der Strukturierung der Implantationsgebiete durch übliche Maskierungsverfahren sowie in der gezielten und reproduzierbaren Beeinflussung der Form und Eindringtiefe des Dotierprofils. Ein entscheidender Nachteil ist die Beschädigung des Silizium Grundmaterials durch den Ionenbeschuss. Für die Halbleitertechnologie kommt es durch diese Kristalldefekte zu negativen Auswirkungen auf die elektrische Aktivität der Verarmungszonen sowie auf die Diffusionseigenschaften der Dotieratome.
In der vorliegenden Arbeit wird die Entstehung von Silizium Kristalldefekten nach einer hohen Bor Implantation und anschließender Diffusion beim Herstellungsprozess von 6-inch Wafern der Infineon Technologies AG untersucht. Besonderes Augenmerk wurde auf den Einfluss der Parameter Implantationsdosis, Implantationsenergie, Beamstrom und verschiedener Diffusionsprozesse auf die Defektentstehung gelegt. Es wurden mit verfügbarer Software numerische Simulationen durchgeführt, in denen diese Parameterwerte variiert wurden. Auf Grund dieser Ergebnisse sowie durch Gespräche mit Experten konnten neue Experimente festgelegt werden. Die Ergebnisse dieser Experimente wurden ausgewertet und mit Literaturwerten verglichen. Zusätzlich wurde der Einfluss einer Silizium Getterschicht an der Waferrückseite und der Einfluss eines höheren Sauerstoffgehaltes im Silizium Grundmaterial auf die Defektenstehung untersucht. Im Zuge dieser Arbeit konnte auch eine bekannte Messmethode dahingegen modifiziert werden, dass erstmals die Verteilung der Kristalldefekte am ganzen Wafer dieser Serie in kurzer Zeit nachgewiesen werden kann.

Um den Leser einen guten Überblick des Gesamtprozesses bis hin zur Defektentstehung zu vermitteln, wurden am Beginn der Arbeit die Grundlagen der Halbleiterverfahrenstechnik kurz beschrieben, die einzelnen angewandten Messmethoden erklärt und die wichtigsten Prozessschritte grafisch übersichtlich dargestellt. Abschließend findet sich ein Kapitel über den theoretischen Hintergrund der Ionenimplantation. Voraussagen der Theorie über die Defektentstehung und Reichweitenverteilung von implantierten Ionen wurden mit den Ergebnissen der Simulationen und Experimenten verglichen und ausgewertet.

Contents

1 Problem description

Investigation of Si crystal defects caused by boron doping

In silicon processing technology one of the most important objectives is to achieve a controlled impurity doping in the crystal. Ion implantation is one of the most important steps to introduce a desired impurity into Si. The disadvantage of implantation is the crystal damage caused to the Si substrate by incident ions. Point defects and defect complexes present in the crystal, significantly influence the electrical activity and the diffusion properties of the dopant.
In this paper the influence of high boron implantation and diffusion processes on crystal defect generation will be investigated. Solutions to decrease or eliminate the crystal defects will be provided and evaluated.

Main areas of experimental investigations

- Influence of different boron diffusion processes
- Influence of boron implantation dose, implantation energy, beam current

Additional areas of investigation (time dependent)

- Si backside getter layer
- Oxygen concentration in Si raw material

2 Basics of semiconductor technology processing

2.1 Base material

Polycrystalline silicon is the basic material from which crystalline silicon is grown. A polycrystall is a solid state body consisting of many small crystallites which are separated from each other through grain boundaries.

In microelectronic fabrication, two main techniques are used for growing crystalline silicon:

1. Czochralski growth
2. Float zone growth

It would be beyond the scope of this paper to describe the two techniques in detail, but it is important to compare the differences in outcome.

Comparison of Czochralski-grown (CZ) and float zone-grown (FZ) material:

Float zone-grown

- Low contamination regarding carbon, oxygen and metals
- ρ can reach values of up to 30000 $\Omega\ cm$
- Crystal structure is very refractory, has a bad getter effect, and breaks easily

Czochralski-grown

- $C < 3 \cdot 10^{16}\ cm^{-3}$, $O = 3 - 5 \cdot 10^{17}\ cm^{-3}$
- $\rho < 50\ \Omega\ cm$
- Stable structure due to SiO_2
- Metallic contaminations depend on the vessel containing the liquid Si

Therefore, the O and C contamination in Silicon is higher in Czochralski-grown silicon because of chemical reactions between the melted silicon and the vessel containing it (see fig. 1) [1].

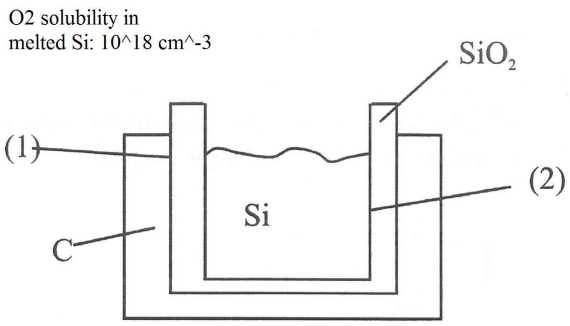

Fig. 1: In Czochralski-grown silicon contamination occurs due to chemical reactions between the silicon and the vessel material.

Chemical reactions:

$$(1)\ C + SiO_2 \rightarrow CO + SiO \tag{1}$$

$$(2)\ CO + SiO \rightarrow SiO_2 + C \tag{2}$$

It is difficult to use FZ-material for wafers with a diameter greater than 150 mm. Temperature strains lead to severe mechanical warping and dislocations because the transition from elastic to plastic deformation occurs only at very high temperatures for the FZ-material.
With CZ-material, on the other hand, microscopic SiO_2 clusters form due to the higher oxygen concentration (Fig. 2). These clusters lower the critical shearing forces by forming dislocations. Additionally, these dislocations perform a gettering function for metallic contaminations [1]. The positive influence upon defect reduction of the SiO_2 clusters has been directly confirmed by our experiments. The results are shown in sec. 5.2.8.

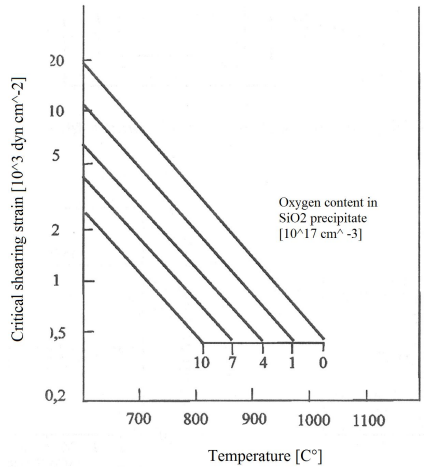

Fig. 2: Critical shearing forces in Czochralski-grown material as a function of temperature and oxygen content.

2.2 Implantation

Through doping, certain elements are brought into the semiconductor substrate of a wafer with the purpose of creating n-type or p-type areas. Common dopants for silicon are P and As to create n-type areas and B to create p-type areas in the substrate. This doping process takes place in defined areas with a defined doping concentration and has to be reproducible. The range distribution of the dopants can be calculated using Fick's laws of diffusion [2].

The process of ion implantation

In the process of ion implantation, atoms or molecules are ionized and subsequently accelerated in an electrostatic field. After passing through various components of a complex system, (e.g. beam analysis magnet, shutter, filter, quadrupole lens, scanner, correction lenses, acceleration- deceleration columinator, final energy filter and beamline isolation chamber), the ions finally strike the surface of a wafer and are thereby implanted into it. The implantation depth depends on the kinetic energy of the ions, on the mass of the implanted ions as well as on the mass of the atoms of the substrate. [2], [3]

The **implantation depth** is controllable by varying the electrostatic field which leads to a change of kinetic energy in the ions. Ion energies range from 10 keV up to several MeV for forming deep structures. The **dose rate** of the ion beam can be controlled either by varying the amount of gas in the ionization chamber (arc chamber) or by varying the amount of primary electrons produced in the arc chamber which ionize the gas in the chamber. With an increasing dose rate higher defect concentrations are usually obtained. An increase of the implantation temperature leads to two outcomes: First, the radiation damage anneals partly or even completely during implantation. Second, the amplitude of lattice vibrations increases, which leads to an increase of the number of ions scattered at the surface. [3], [2], [4]

2.3 Diffusion - oven processes

Diffusion is an expansive field in semiconductor fabrication and it would be far beyond the scope of this thesis to discuss every step of the process flow in the category of diffusion or oven processes. Therefore, I will focus on processes that through discussions with experts, were found to be of importance for this thesis. These are: Fick's laws of diffusion, diffusion mechanisms and process flow.

Fick's first law

The basic equation that describes diffusion is Fick's first law. It is used when the concentration within the diffusion volume does not change with respect to time ($J_{in} = J_{out}$) and is in one dimension:

$$J = -D\frac{\partial c(x,t)}{\partial x} \tag{3}$$

with

J ... diffusion flux in dimensions of $\frac{mol}{m^2 \cdot s}$

D ... diffusion coefficient in dimensions of $\frac{m^2}{s}$

c ... doping concentration in dimensions of $\frac{mol}{m^3}$

x ... position (length)

Therefore, according to Fick's first law, the diffusion flux is proportional to the concentration gradient against the direction of the diffusion ($\partial c\ mol/\partial x\ m^{-4}$). The proportion constant is the **diffusion coefficient** which is proportional to the velocity of the diffusing particles, which depends on the temperature and the size of the particles according to the Stokes-Einstein relation.

In three dimensions for an isotropic medium, Fick's second law, which describes the change in concentration, is applied:

$$\frac{\partial c}{\partial t} = D\frac{\partial^2 c}{\partial x^2} \tag{4}$$

To solve this second order differential equation, knowledge of at least two independent boundary conditions is required. A discussion of the solution to this differential equation would be beyond the focus of this paper and the reader is referred to [5].

For cubic crystals D is anisotropic and the temperature dependence of the diffusion coefficient is demonstrated through an Arrhenius equation:

$$D = D_0 \cdot e^{-\frac{W}{kT}} \tag{5}$$

with

k ... Boltzmann constant

T ... absolute temperature

W ... activation energy for a jump from one lattice site to the next

D_0 ... material constant

For B in Si the material constant D_0 is 0.037 cm^2/s and its activation energy of the intrinsic diffusivity E_{ia} is 3.46 eV. D_0 is mostly independent from the temperature and mainly depends on the vibration frequency of the Si-lattice and its geometry. [5] [1]

Diffusion mechanisms

In an atomistic model of diffusion, the lattice sites in a crystal are represented as the minima of parabolic potential wells. At temperatures above absolute 0 atoms oscillate around their equilibrium position. When an impurity atom is implanted into this crystal it may sit between lattice sites in an interstitial position. Atoms that do not bond immediately with the crystal lattice are typically **interstitial impurities**. They diffuse rapidly but do not directly contribute to doping because they are electrically inactive. Another type of impurity is one which replaces the Si atom on the lattice site and is called **substitutional impurity**. In order for a substitutional impurity to move in the crystal it must overcome the potential well in which it rests. For a direct exchange to take place (see fig. 3 (a)), at least six bonds must be broken for the host atom and the impurity atom. For a vacancy exchange to occur (see fig. 3 (b)), only three bonds must be broken and this mechanism is therefore one of the dominant diffusion mechanisms. **Interstitialcy diffusion** can occur in the presence of silicon self-interstitials as shown in fig. 3 (c). Hereby, an interstitial silicon atom displaces the impurity, driving it into an interstitial site. From there it moves rapidly to another lattice site, where the silicon atom is removed to an interstitial site again.

In the **Frank-Turnbull method** as shown in fig. 3 (d), the interstitial impurity is captured by a vacancy. In the **kick-out mechanism**, the impurity replaces a lattice atom. The two mechanisms are different from the interstitialcy method in that they do not require the presence of self-interstitials to drive the process. [5]

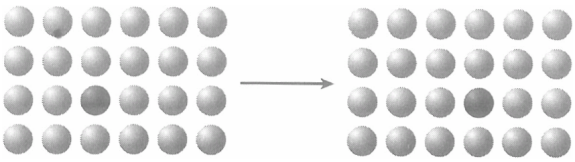

(a) Direct exchange. Diffusion of an impurity atom by direct exchange.

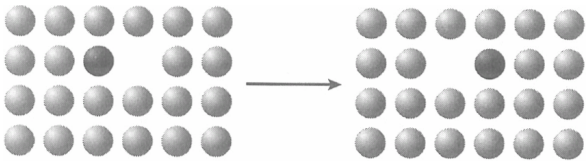

(b) Vacancy exchange. Diffusion of an impurity atom by vacancy exchange. This type is much more likely then (a) because of the lower energy required.

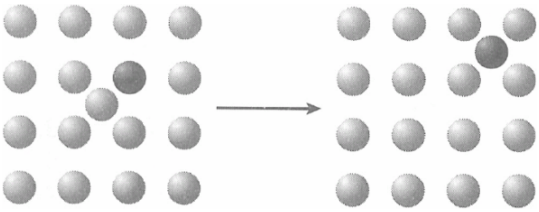

(c) Interstitial diffusion. An interstitial Si atom displaces a substitutional impurity, driving it to an interstitial site where it diffuses some distance before it returns to a substitutional site.

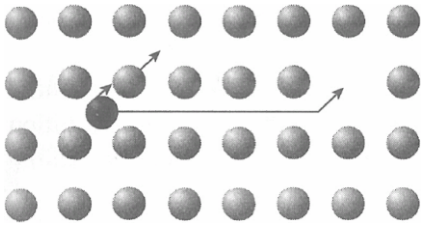

(d) The kick-out (left) and Frank-Turnbull mechanisms (right).

Fig. 3: Four different atomistic models of diffusion are represented schematically above according to [5].

Process flow

The goal in the semiconductor production process is to create a preferably rectangular doping profile. To achieve that, the diffusion process with its parameters 'dose' and 'depth' is divided into a two-step process, firstly a **predeposition diffusion** and secondly the **diffusion process** itself. [1]

Given a fixed ion source at the surface for all times greater than zero, the boundary conditions for equation 4 for the predeposition diffusion are $c(x = 0, t) = const = c_0$ $(solubility)$. The solution for these conditions is given by [1]:

$$c(x,t) = c_0 \cdot erfc(\frac{x}{2\sqrt{Dt}}) \tag{6}$$

with:

$$erfc(x) = 1 - \frac{2}{\sqrt{\Pi}} \int_0^x \exp^{-\frac{1}{2}\xi^2} d\xi \tag{7}$$

The complimentary error function can be found in many math handbooks for various values. C_0 is the fixed surface concentration which only slightly depends on the temperature. To ensure a specific C_0 at the surface, an oxide is deposited, which leads to diffusion from the solid phase. $2\sqrt{D \cdot t}$ is known as the characteristic diffusion length. It includes temperature and time as parameters. Typical values for the temperature are between 900℃ and 1250℃.

The **predeposition diffusion** leads to a very steep doping profile. Often the goal is to reduce the high dopant concentration near the surface and instead distribute it deeper and more evenly into the substrate and is done during the **diffusion process**. This is achieved by adding an SiO_2 layer at the wafer surface to ensure that dopants cannot diffuse in or out of the substrate (see e.g. fig 12). Typical temperatures and times as well as doping profiles before and after diffusion can be seen in sec. 4.5. A standard doping profile after boron implantation and diffusion is shown below in fig. 4.

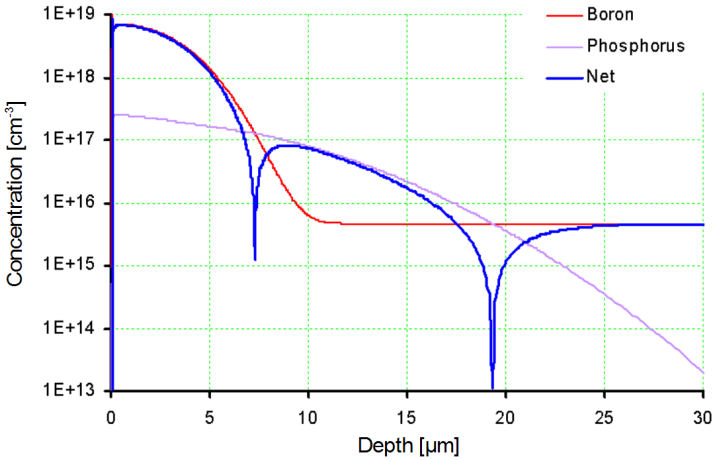

Fig. 4: A standard doping profile after boron implantation and diffusion is shown above. The two minima of the net value occur as expected at the p-n-junctions.

2.4 Lithography and etching processes

For the study of crystal defect generation, lithography and etching processes have been identified as low contributors to the formation of crystal defects. Therefore, a description of these processes would be beyond the scope of this paper and will not be discussed here. For the interested readers I would refer them to the works of [5] and [2].

2.5 Chemical cleaning processes

The same identification as described in section 2.4 has been made for chemical cleaning processes and will therefore not be discussed here either. For the interested reader I would refer to the works of [5] and [1].

2.6 Methods for crystal defect detection and analysis

Four different methods for analysing defects in a wafer were used. All of the results differed from one another while the secco etch solution provided the clearest results. Below is a brief description of each of the four methods:

2.6.1 ELYMAT measurement

The ELYMAT (short for Electrolytical Metal Tracer) technique allows a fully automated mapping of the minority carrier diffusion length (life time) with a sufficient lateral resolution. The Si wafer is located in an electrolytical double cell and is in contact with a suitable electrolyte on the front- and backside. A laser beam scans the wafer thereby locally generating minority carriers which lead to a diffusion current (photo current). Depending on the measuring mode, the diffusion current can be measured on the frontside or backside of the wafer.
Crystal defects or contaminations in the wafer lead to a reduction of the diffusion current due to recombinations of the minority carriers. The recombination behavior depends on the depth position of the defects or contaminations, if recombination at the surface can not be neglected or if the depth distribution of recombination centers is not uniform. Therefore, the diffusion current contains information about the surface recombination velocity on the front- and backside as well as about the depth dependence of the diffusion length. [6]

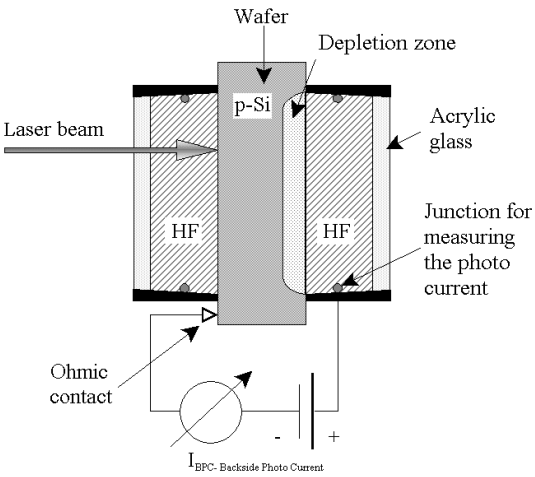

Fig. 5: Schematic illustration of the electrolytical double cell of the ELYMAT.

2.6.2 Poly measurement

To highlight defects on the wafer surface, a polysilicon layer is precipitated onto the wafer. In so doing, the defects are easier to see and can be observed through either optical microscopy or scattered laser light detection.

2.6.3 Vapour phase decomposition (VPD) using atomic absorption spectroscopy

Contamination can be found mainly on the surface of a wafer. To analyse the concentration of the contamination, the wafer is put into an environment containing HF gas. The HF gas condenses on the wafer where the surface contamination dissolves into the HF droplets. These droplets are then pipetted off and analysed using atomic absorption

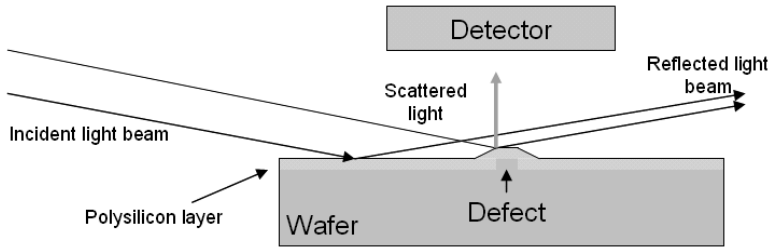

Fig. 6: Schematic description of the detection of suface defects using scattered laser light. To highlight defects, a polysilicon layer has been precipitated onto the wafer.

spectroscopy [1].
With this method, light containing different wavelenghts with a specific intensity is passed through the sample containing the contamination. If the energy of the light corresponds to the energy difference between two energy levels of electrons in an atom, part of the light will stimulate the electrons and raise them to the higher level. Therefore, a portion of the light is being absorbed and its intensity weakened while passing through the sample. The intensities before and after passing through the sample are measured and compared. Using the Beer-Lambert law, the relationship between the concentration of atoms, the distance the light travels through the sample and the portion of light that is absorbed can be determined. A more detailed description of atomic absorption spectroscopy would be beyond the scope of this paper and I would refer the reader to [7].

2.6.4 Secco etch solution

To highlight defects in the wafer, defect selective etching is used. As is the case in our experiment, defects that can't be seen before etching are often easily observable using simple optical microscopy after etching. If there aren't too many defects on the surface, the defect density can be determined by counting them [5].

Etching methods

In silicon processing technology, wet chemical etching processes as well as dry or plasma etching processes are used. With wet chemical etching processes the wafer is simply immersed in a solution that reacts with the exposed film. It is difficult to control this process for several reasons. Primarily because high level defects tend to occur due to contamination in the solution, it can't be used for small features and it produces large volumes of chemical waste. Specifically-developed dry- or plasma-etching processes are well-suited for bringing forward in the wafer the precise structures that are necessary. Some of the advantages compared to wet etching are that plasmas are easier to start and stop, plasma etch processes are less sensitive to small changes in the wafer temperature,

and they produce less chemical waste than wet etching. [2], [5]

Generally, etching processes are divided into **isotropic** and **anisotropic** processes [2]:

- The isotropic etching process removes the substrate material uniformly in all spatial directions. This leads to an undercut of the etching mask.
- The anisotropic etching process removes the substrate material perpendicular to the surface of the wafer only. The etching mask is conveyed with high accuracy into the layer beneath it.

After testing these four different methods, the use of a Secco etch solution turned out to be the most effective. It is a wet chemical etching process which delineates oxidation-induced stacking faults in (100) silicon and is applied in our production process immediately after the diffusion process (see sec: 2.6).

Secco etch solution:

$$2:1;\ HF/K_2Cr_2O_7\ (0.15molar)$$

2.6.5 NSX automated defect-inspection system

Instead of a manual visual inspection of the wafers and dies at the tail end of semiconductor production (performed by inspectors with microscopes), an automated vision-based system is used. It can detect defects down to one half micron. The system's vision process uses a black and white area-scan CCD camera which operates in continuous-light, as well as electronic shutter or strobe modes as the wafer moves back and forth on the stage. A second color CCD camera provides in-line defect review displayed on a monitor.
Before inspection begins, a wafer setup has to be made and must include identification information, wafer and die size, die pitch, whether there's a notch or flat on the wafer, as well as the location of features like alignment marks.
The core functionality of the inspection system is based on a 'reference wafer' which is used for comparison. The system's detector is trained by building a mathematical model (reference wafer) of a die to which all the production die are compared. This model is constructed by selecting $30 - 40$ dies that are known to be good. The data from those good dies is used in the NSX for the creation a statistical pixel mode of a perfect die against which all the dies for inspection are contrasted. [8]

3 Production process of 6-inch wafers of the technology being investigated

The following list gives a brief description of the individual steps of the production process up to when defects start to occur. It is important to keep in mind that the following list does not represent the entire production process but only the individual processes which are relevant to the analysis of the defects which occur.

The base material consists of silicon doped with oxygen and boron:

Si Concentration: $5 \cdot 10^{22}\ cm^{-3}$

O_2 Concentration: $3 \cdot 10^{17} - 5 \cdot 10^{17}\ cm^{-3}$

B Concentration: $3 \cdot 10^{15} - 5 \cdot 10^{15}\ cm^{-3}$

1. Cleaning of the base material.

Fig. 7: Cleaned base material.

2. Oxidation of a 1300 nm primary oxide layer at 1100°C.

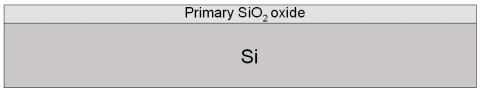

Fig. 8: Primary oxide layer on the base material.

3. Removal of the primary oxide through various processes at specific areas for the upcoming phosphorus implantation.

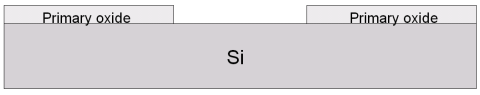

Fig. 9: Primary oxide has been removed in certain areas where phosphorus implantation will be carried out.

4. Phosphorus implantation at a voltage of 80 keV. Implanted phosphorus dose: $2 \cdot 10^{14}\ cm^{-2}$.

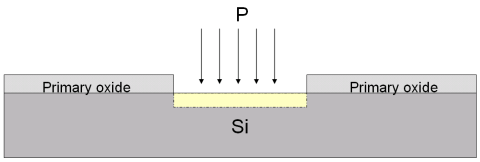

Fig. 10: Phosphorus implantation.

5. Phosphorus diffusion at 1250℃ for approximately 24 hours.

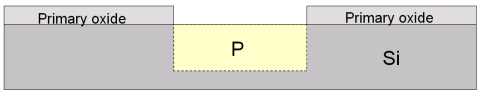

Fig. 11: The implanted phosphorus layer undergoes diffusion at $T = 1250$℃ for approximately 24 h to be destributed more deeply and more evenly into the wafer.

6. Removal of the primary oxide and oxidation of a 100 nm wet oxide layer at 975℃.

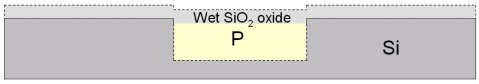

Fig. 12: The primary oxide has been removed and a SiO_2 layer is added using a wet oxidation technique.

7. A resistance coating is added to protect certain areas before starting the boron implantation. Boron implantation is done at a voltage of 80 keV with an implantation dose of $2.5 \cdot 10^{15}$ cm^{-2}.

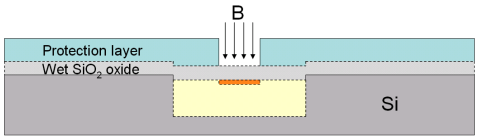

Fig. 13: Boron implantation.

8. Diffusion of the implanted boron layer at 1150℃ for 920 min.

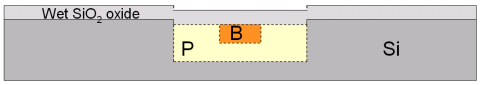

Fig. 14: The implanted boron layer undergoes diffusion at $T = 1150$℃ for 920 min to be destributed more deeply and more evenly into the wafer.

9. The SiO_2 layer is removed using a wet chemical etching method. Afterwards the wafer is cleaned through a wet chemical cleaning.

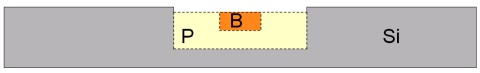

Fig. 15: The SiO_2 layer has been removed using a wet chemical etching method and the wafer has been cleaned with a wet chemical cleaning.

4 Simulations

All the simulations were done using ICECREM for WINDOWS, Version 4.3. The following parameters were used as constants in all the simulation models:

Substrate	
Orientation of the substrate:	100
Concentration of doping element:	$4.56 \cdot 10^{15}\ cm^{-3}$
Doping element:	Boron
Specific resistivity:	3 Ohm cm
Wafer thickness:	400 μm
Grid	
Grid spacing:	10 nm
Depth of the simulation area:	15 μm
Deposit	
Total oxide thickness:	0.1 μm

Given these parameters we are left with a model as illustrated in fig. 16. Based on that model, the following three variations of parameters will firstly be simulated and later be experimentally tested and analysed:

1. Variation of the energy from $10 - 160\ keV$ before and after diffusion (see sec. 4.2, 4.3).

2. Variation of the doses from $1.0 \cdot 10^{14} - 5.0 \cdot 10^{15}\ cm^{-3}$ (see sec. 4.4).

3. Combined simulation with a split in doses and diffusion time (see sec. 4.5).

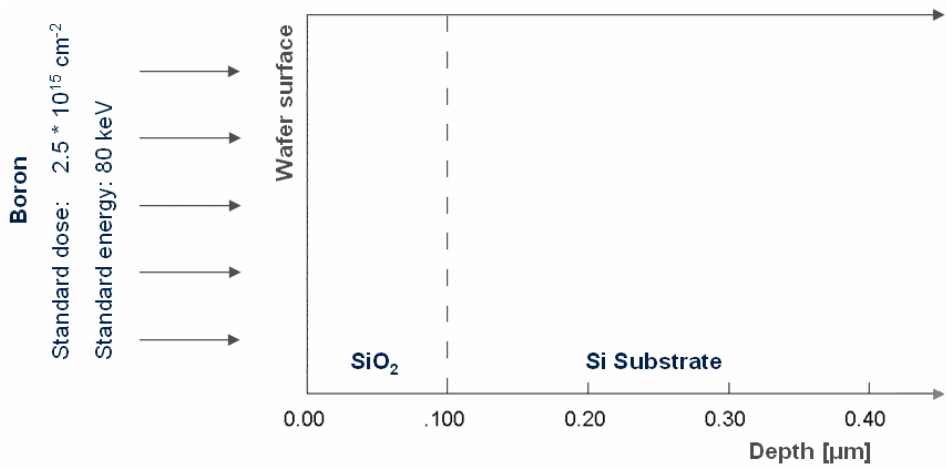

Fig. 16: Model for simulations.

4.1 Distribution of boron after implantation

According to the LSS-theory, implanted boron ions posses a Gaussian range distribution around an average project range R_p as discussed in section 6.2. Because the theory only considers amorphous medium and because in our case we are dealing with a crystal substrate structure covered with a 100 nm amorphous oxide layer through which the boron ions are implanted, we wanted to be able to compare the LSS model with our real-life implantation process. We ran a simulation with no diffusion after implantation. Our simulation values were:

Element: Boron
Energy: 80 keV
Dose: $2.5 \cdot 10^{15}\ cm^{-2}$

Although our real-life implantation differs in many ways from the simplifications the LSS-theory has to make, our results, shown in fig. 17, are very similar to the predictions of the LSS theory. The maximum of the projected range R_p is at a depth of 0.2683 μm with a standard deviation $\Delta R_p = 0.0734$. The discontinuity of the graph at the SiO_2/Si boundary layer occurs due to software calculations, which don't take into account boundary layer effects but instead calculate the distribution seperately for the SiO_2 layer and the substrate.

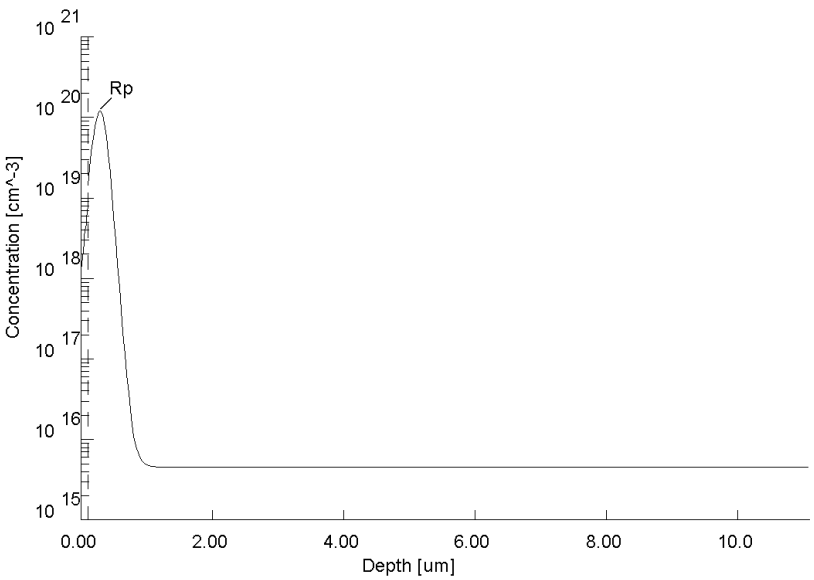

Fig. 17: Boron profile after implantation. Distribution of implanted boron ions at $V = 80\ keV$ and a dose rate of $2.5 \cdot 10^{15}\ cm^{-2}$. The boron is implanted through a 100 nm oxide layer and has its maximum at a depth of approximately $0.27\mu m$. The Gaussian range distribution around an average project range R_p, as well as the location of its maximum, are in accordance with the LSS theory described in section 6.2.

4.2 Variation of the implantation energy from $10 - 160\ keV$

In the next step, we simulated the maxima of the projection range R_p and its standard deviation ΔR_p for different implantation energies using the standard dose in the current production process of $2.5 \cdot 10^{15}\ cm^{-2}$. Our simulation values were:

Element: Boron
Energy: Ranges from $10 - 160\ keV$ as shown in fig. 18.
Dose: $2.5 \cdot 10^{15}\ cm^{-2}$

The red horizontal line in fig. 18 marks the SiO_2/Si boundary layer. According to the results of the simulation, implantation energies that are equal to or higher than approximately 40 keV propel the maximum of the projection range R_p inside the substrate if the standard deviation ΔR_p is taken into account. Experiments that analyze the relationship between the projection range R_p and the crystal defect concentration after the diffusion process will be discussed later.

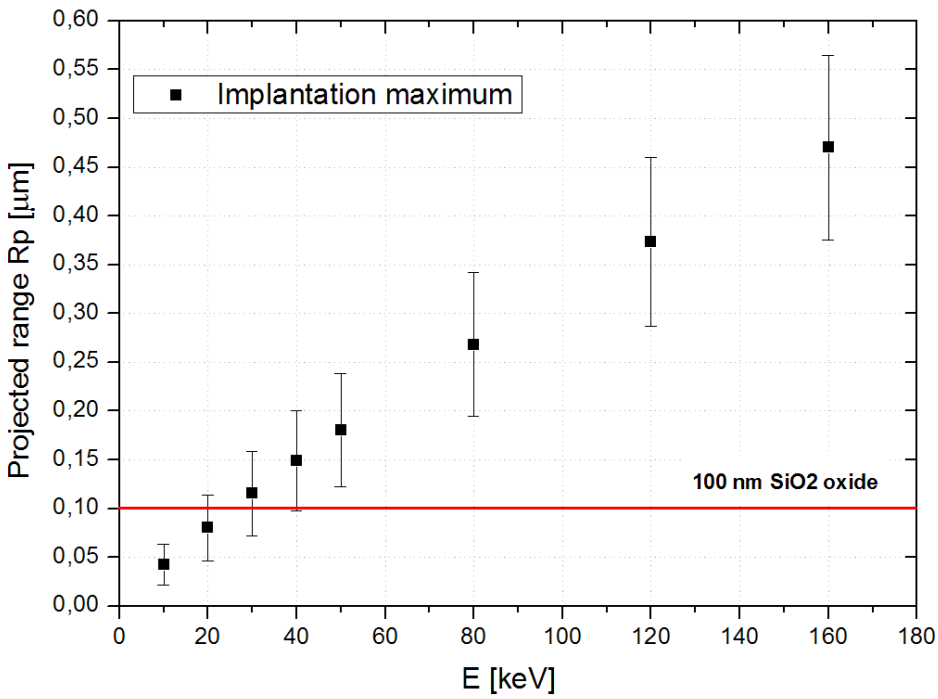

Fig. 18: Boron implantation maxima before diffusion. The implantation maxima and its standard deviation ΔR_p of the implanted boron ions before diffusion in the wafer for different implantation voltages are shown above. The red horizontal line shows the end of the 100 nm oxide layer and the beginning of the wafer material beneath it. The simultaion is based on a constant dose rate of $2.5 \cdot 10^{15}\ cm^{-2}$. The standard process used in the current production process of 6-inch wafer, where crystal defects occur, uses a voltage of 80 keV.

4.3 Variation of the implantation energy from $10 - 160\ keV$ - effects after diffusion

Before looking at the effects of different implantation energies on the boron distribution after diffusion, it is useful to first understand the effect of the diffusion process upon the boron distribution in the wafer. To enable that more easily we ran a simulation based on a standard production process. Our standard simulation values were:

Implant	
Element:	Boron
Energy:	$80\ keV$
Dose:	$2.5 \cdot 10^{15}\ cm^{-2}$
Oxidize	
Temperature:	1150°C
Time:	920 min
Mode:	Inert ambient

The result of the standard process is shown in fig. 19. To understand the effect of the diffusion process, figure 19 must be compared with figure 17. The scaling of the two figures has purposefully been made equal to visualize how the narrow Gaussian distribution after the boron implantation changes to a broad, exponentially decreasing distribution due to the diffusion process. After diffusion the boron ions reach a depth of almost $10\ \mu m$.

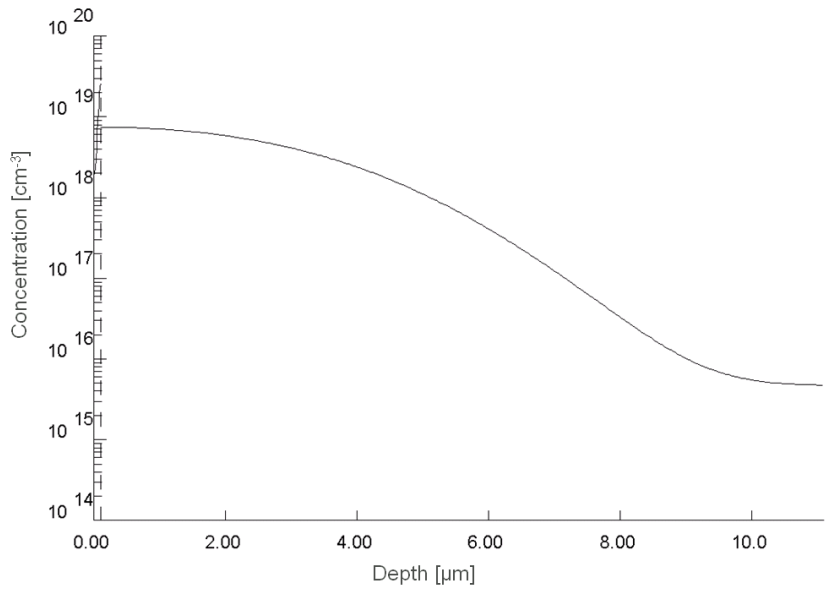

Fig. 19: Boron profile after diffusion. Standard values of the production of the technology being investigated have been used. These are: 100 nm oxide layer, 80 keV implantation energy, $2.5 \cdot 10^{15}\ cm^{-2}$ implantation dose, 1150°C diffusion temperature for 920 min. Compared with fig. 17, the effect of the diffusion process can be clearly seen. While the integral under the curve remains the same (because the same dose rate has been implanted) the narrow Gaussian distribution in fig. 17 changes to an exponentially decreasing distribution. The boron ions reach a depth of almost $10\ \mu m$ after diffusion.

To understand the influence of the implantation energy upon the boron distribution in the wafer after the diffusion process, we simulated boron implantation using different energy values ranging from $10 - 160\ keV$ as shown in fig. 20. The implantation dose used for these simulations was $2.5 \cdot 10^{15}\ cm^{-2}$ and was chosen based on the current standard dose in the production process of the 6-inch wafer being investigated. The same principle was applied for the implantation values which are $T = 1150$℃ and $t = 920$ min. As can be seen in fig. 20, the boron concentration in the oxide layer and substrate change with an increase in energy while the total concentration must of course remain constant. With an increase of implantation energy, the implantation range R_p naturally increases (see fig. 18). This leads to a decrease of the boron charge in the oxide layer after diffusion.

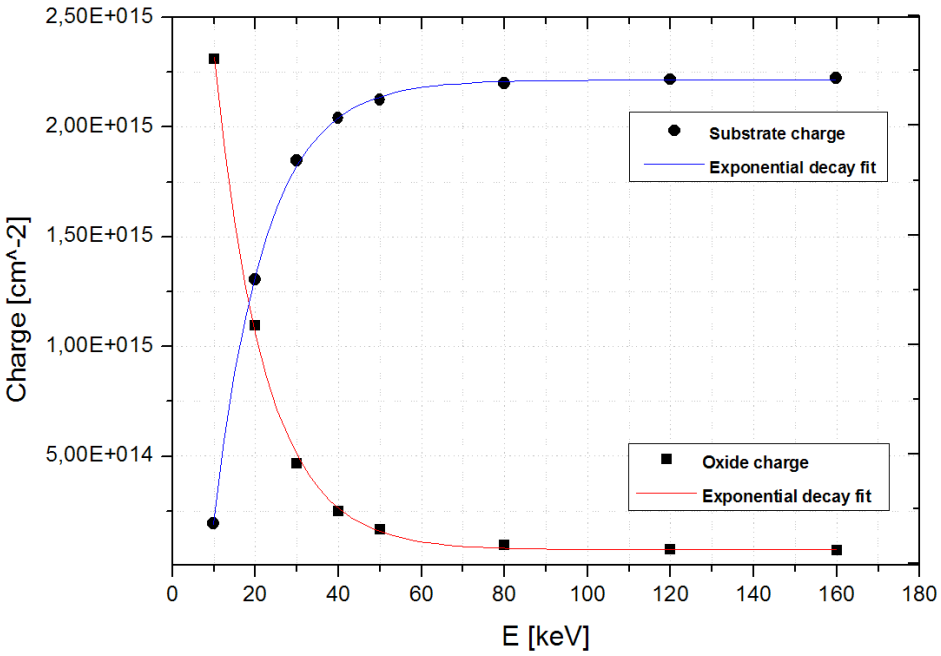

Fig. 20: Boron concentration in the oxide layer and substrate after diffusion. The two graphs show the charge of the implanted boron in the 100 $nm\ SiO_2$ layer as well as in the silicon beneath it. Constant parameters for the simulations are an implantation dose of $2.5 \cdot 10^{15}\ cm^{-2}$ and a diffusion temperature and time of 1150℃ for 920 min. With an increase in voltage, the boron is implanted deeper into the substrate, thus increasing the charge in the oxide layer and increasing the charge in the silicon wafer.

4.4 Variation of the doses from $1.0 \cdot 10^{14} - 5.0 \cdot 10^{15}\ cm^{-3}$

With any given implantation dose, the distribution of the total boron concentration in the SiO_2 layer and oxide becomes different after the diffusion process. In this simulation we tried to understand how the distribution changes depending on the total implanted boron concentration. Our simulation values were:

Implant

Element: Boron

Energy: 80 keV

Dose: Ranges from $1.0 \cdot 10^{14} - 5.0 \cdot 10^{15}\ cm^{-2}$ as shown in fig. 21.

Oxidize

Temperature: 1150°C

Time: 920 min

Mode: Inert ambient

The results show that with an increase in the total implantation dose, the increase in the SiO_2 layer and the oxide do not grow at the same rate. In fact, with an increase in the total implantation dose, the percentage of the implanted boron in the SiO_2 layer decreases and the percentage in the substrate beneath it increases compared to the total percentage.

For doses marked with (1), (2) and (3) in fig. 21, experiments were carried out and analysed for crystal defects. Only in (1), implantation dose: $2.5 \cdot 10^{15}\ cm^{-2}$, did no defects occur. A more detailed discussion of these results will follow.

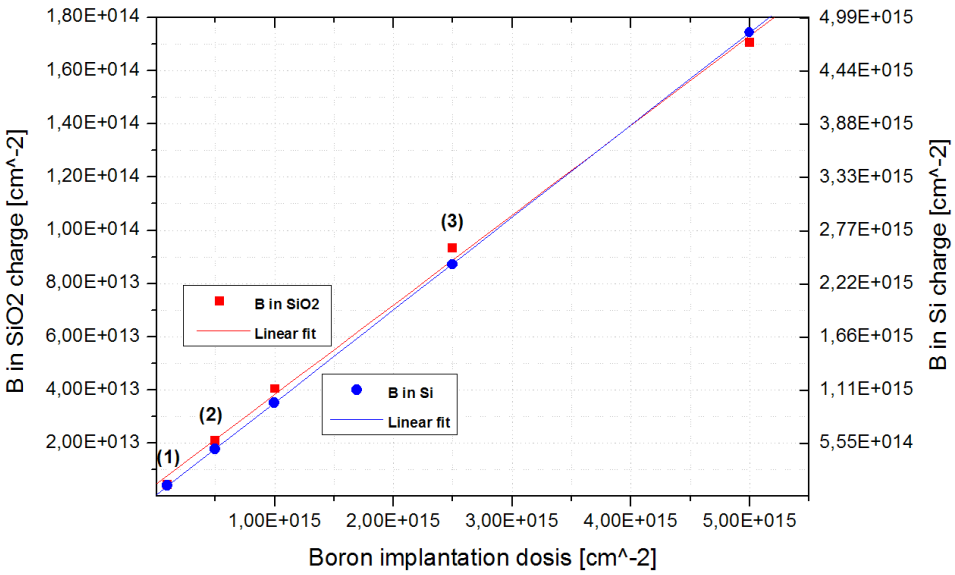

Fig. 21: Change of boron concentration in the oxide layer and the substrate for different implantation doses. The boron charge in the SiO_2 layer and the silicon underneath it is shown based on different implantation doses. Constant parameters for the simulations were an implantation energy of 80 keV, a 100 nm oxide layer and a diffusion temperature and time of 1150°C for 920 min. For values (1), (2) and (3) experiments were carried out and will be discussed later, the other two values were only simulated.

4.5 Combined simulation with a split in doses and diffusion times

In our last simulation, the goal was to implant using a lower implantation dose by splitting the standard implantation dose and process into three steps. In each step we only implanted a third of the standard implantation dose followed by a short period of diffusion. After the third step the diffusion time was adjusted in such a way that the total diffusion time added up to the 920 min of the standard process. In total, the implanted dose and time matched the standard process which allowed us to effectively compare the data.

With a lower implantation dose, fewer collision cascades occurred, which might lead to fewer crystal defects. Although our simulation wasn't able to determine the amount of crystal defects, it allowed us to check if the final boron distribution after the entire process matched the required distribution of the standard process. An experiment was carried out in order to compare the crystal defect formation to the standard process.

Our simulation values were:

Implant		**Oxidize**	
Element:	Boron	Temperature:	1150℃
Energy:	80 keV	Time:	15 min
Dose:	$8.33 \cdot 10^{14}\ cm^{-2}$	Mode:	Inert ambient
Implant		**Oxidize**	
Element:	Boron	Temperature:	1150℃
Energy:	80 keV	Time:	15 min
Dose:	$8.33 \cdot 10^{14}\ cm^{-2}$	Mode:	Inert ambient
Implant		**Oxidize**	
Element:	Boron	Temperature:	1150℃
Energy:	80 keV	Time:	890 min
Dose:	$8.33 \cdot 10^{14}\ cm^{-2}$	Mode:	Inert ambient

A comparison between the boron profile of the combined simulation shown in fig. 22 and the standard process boron profile simulation shown in fig. 19 showed almost no difference in its distribution. Therefore this process was used as a defined experiment to analyze its defect formation.

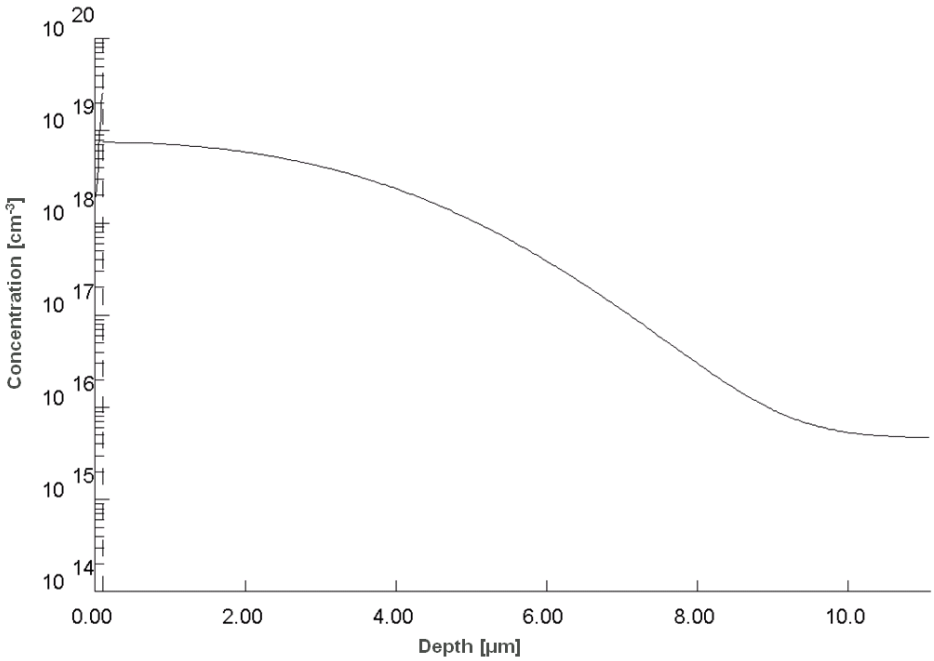

Fig. 22: Boron profile after a combined simulation with a split in doses and diffusion times. The entire process was split into three steps. In each step we only implanted a third of the standard implantation dose followed by a short period of diffusion. After the third step the diffusion time was adjusted in such a way that the total diffusion time added up to the total time of the standard process. The detailed implantation and diffusion parameters for this simulation are listed above.

5 Defined experiments and observations

In this section the experiments conducted and the results found within this thesis will be discussed. The methods used for detecting the findings of the experiments have been explained in sec. 2.6 and will be referred to intermittingly.

5.1 Defined set of experiments

A set of experiments was defined based on the simulations in sec. 4.5 as well as on discussions with experts in the field of semiconductor fabrication. For the purpose of a total overview of the conducted experiments with the aim of achieving a decrease in crystal defects in the 6-inch wafer technology being investigated, table 1 has been added. Table 1 lists the entire set of experiments conducted by employees of Infineon Technologies on the topic of crystal defect reduction in the past, including experiments which were conducted before the writing of this paper. The last two columns show which simulations and experiments were carried out by our team during the writing of this thesis, and only those results will be analyzed and discussed in sec. 5.2.

	Work packages	Defect density change	Simulation conducted	Experiment conducted
Base material	Base material with higher O_2 concentration, min $> 3 \cdot 10^{17}\ cm^{-3}$	**decrease**		yes
	Different suppliers: Ocmetic / SEH	no change		
	Floating zone material	no change		yes
Implantation	Frontside Ar damaging before buried conductor implantation	no change		
	Ar damaging before P implantation	no change		
	Boron silicate glass layer (BSG)	ongoing		
	Half beam current	no change		yes
	Increase of the wafer temperature during implantation	open		
	Split dose and diffusion time	**decrease**	yes	yes
	Variation of the implantation energy:			
	Implantation energy: 20 keV	**decrease**	yes	yes
	Implantation energy: 40 keV	**decrease**	yes	yes
	Implantation energy: 150 keV	no change	yes	yes
	Variation of the implantation dose in ascending order	increase	yes	yes
Cleaning	Twofold cleaning process before B diffusion	increase		
Diffusion	Backside getter layer	**decrease**		
	Nitride layer before buried conductor diffusion	increase		
	Rapid thermal processing before buried conductor diffusion	no change		
	Smooth oven processes:			
	Smooth 1: different ramping (600°C) and $O_2 - N_2$ P diffusion	increase		yes
	Smooth 2: N_2 drive before O_2 oxidation during P diffusion	**decrease**		yes
	Smooth 3: $O_2 - N_2 - O_2$ diffusion	no change		yes
	Frontside TEOS layer before buried conductor diffusion	no change		

Table 1: Total overview of experiments which were conducted on the reduction of crystal defects. The column **'work packages'** lists all the experiments within different production steps (see sec. 3) which were conducted on the issue in the past. The **'defect density change'** column shows which experiments led to an improvement and the last two columns show which simulations and experiments have been conducted in the course of this Bachelor's thesis. The results of these experiments will be discussed in sec. 5.2.

5.2 Description of the quantitative results

As discussed in sec. 2.6.4, the use of a Secco etch solution was found to be the most effective way of identifying crystal defects in the wafer. After applying the Secco etch solution, the defects could be easily observed using an optical microscope. To get an overall picture of the defect distribution among the 2136 chips on a 6-inch wafer, NSX scans (2.6.5) were performed and subsequently analyzed. Additionally, a VPD analysis (see sec. 2.6.3) for each lot containing the wafers has always taken into account the concentration of the contaminations which could not be completely eliminated in real-life production. Below are three examples which demonstrate what the results of the analyzing methods generally looked like:

1. Point defects after Secco etching detected through an optical microscope
Figure 23 shows three pictures of single dies from the same wafer taken with an optical microscope. The pictures were taken along the diameter of the wafer starting from the far left to the far right with the second picture being of the center of the wafer. What can be seen is an indication of the uneven distribution of the defects on the wafer. Generally defect formation seems to be higher on the rim of the wafer although unfortunately no specific constant crystal defect distribution can be attributed to the wafers. The rectangle marked with a red circle is the only part of each die that was not implanted with phosphorus. We were able to learn that more defects occur in this specific part of each die than on the rest of the die.

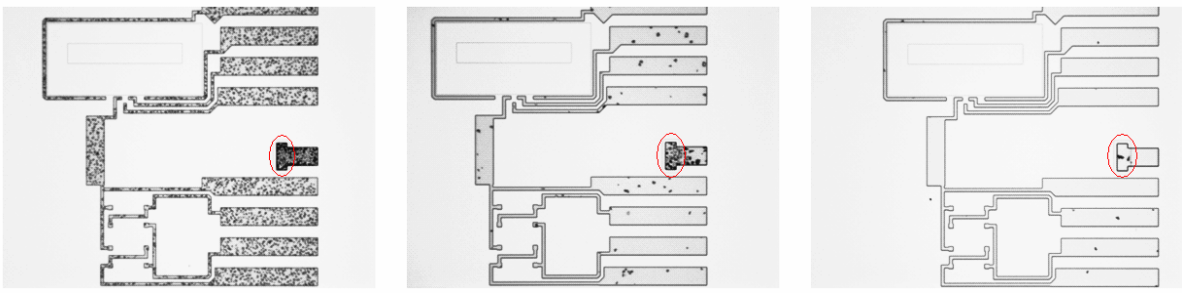

Fig. 23: Defects after Secco etching detected through an optical microscope. The pictures were taken along the diameter of the wafer starting from the far left to the far right with the second picture being of the center of the wafer. The uneven distribution of the defects is very typical for the wafers of the technology being investigated in this thesis. The red circles mark the only part of the chip that was not implanted with phosphorus. Generally an increased defect density can be observed in this area, as is the case in the three pictures above.

2. Defects after Secco etching detected through NSX analysis
Figure 24 shows a typical depiction of a wafer after the NSX analysis. Each wafer contains 2136 chips which are identified as white squares in fig. 24. Instead of viewing the defect details for each chip, the NSX analysis allowed us to determine the defect density distribution within the entire wafer. A general characteristic clearly seen in fig. 24 was the higher defect concentration on the rim of the wafer. This has been observed in most of the wafers analyzed so far. An explanation for this characteristic has not yet

been found. The average defect density of this specific wafer is $77,48\ cm^{-2}$.

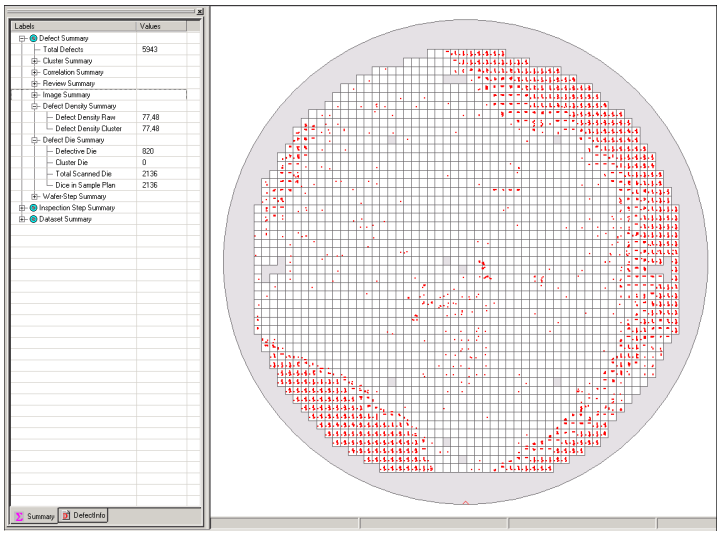

Fig. 24: NSX analysis of a wafer. The white squares indicate the positions of the 2136 chips on the wafer, and the red spots mark defects found through the NSX analysis (see sec. 2.6.5). A general characteristic of defect formation on the 6-inch wafers being investigated is the higher defect concentration on the rim of the wafer. An explanation for this characteristic has not yet been found.

It is very important to keep in mind that the number of defects detected by the NSX strongly depends on the setting of the NSX setup used. **The number of defects detected by the NSX does not reflect the absolute number of defects on the wafer**, but does allow us to determine increases or decreases of defect formation within wafers that have been measured with the same setup.

3. VPD analysis of the concentration of contamination in a lot

The concentration of Al, Ca, Cu, Fe, Ni and Na contamination for each wafer is determined throughout the course of the VPD analysis (see sec. 2.6.3). On a typical VPD chart the y-axis shows the concentration level in cm^{-2}, on the x-axis the different wafers are listed. A VPD chart will be added to every experimental analysis conducted during the writing of this thesis.

Below the results of all the experiments that have been defined in sec. 5.1 and conducted during the course of this paper will be discussed. A list of the defined experiments can be found in the last column of table 1. The results were obtained using the three analyzing methods described in sec. 5.2.
For the purpose of internal Infineon Technologies Austria traceability, a table will be attached containing the lot and wafer numbers next to every graph displaying the results of the experiments.

5.2.1 Variation of the implantation energy

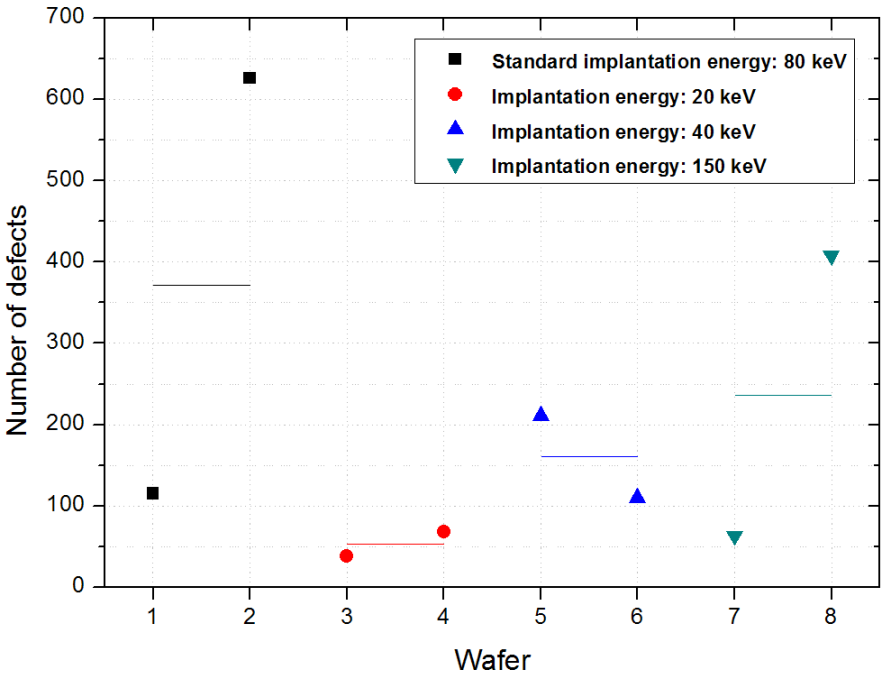

Lot Nr.:	VC815165
X-axis value	Wafer Nr.
1:	10
2:	22
3:	5
4:	19
5:	7
6:	17
7:	4
8:	18

Fig. 25: Number of defects of wafers undergoing different implantation energies.

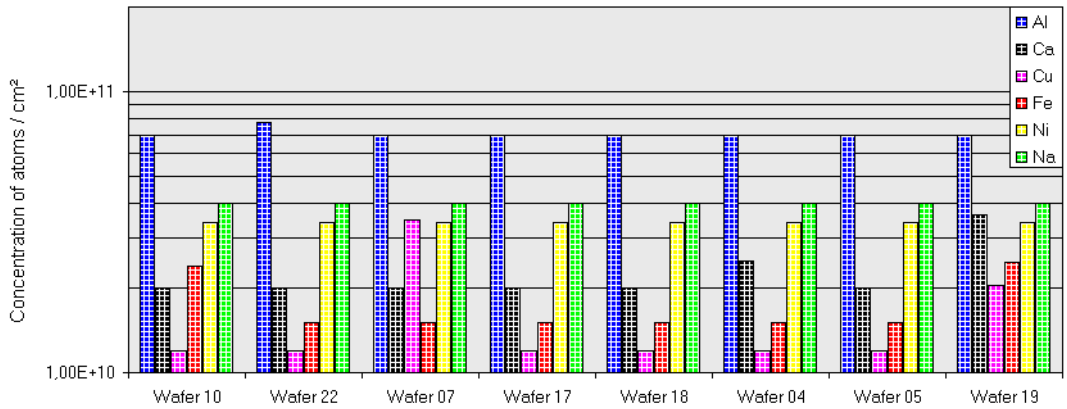

Fig. 26: VPD analysis of wafers exposed to different implantation energies.

In this experiment, the effects of a variation in the implantation energy upon defect formation were studied. Four different implantation energies were chosen: (1.) Standard implantation energy: 80 keV (2.) 20 keV (3.) 40 keV and (4.) 150 keV.
The results show clearly that with an increase in implantation energy, more defects occur. This is probably due to the fact that the most defects occur when the boron distribution after implantation reaches its maximum. Since the SiO_2 layer is removed later on in the production process, the defects with its gettered contaminations in that layer are also gone. With an implantation energy of 20 keV, the maximum of the boron distribution after implantation lies only in the amorphous SiO_2 layer, whereas

an energy of 150 keV, the maximum lies entirely in the wafer material. At 40 keV the implantation maximum lies in the SiO_2/Si boundary layer.
According to the theoretical background of ion implantation, a higher implantation energy **does not** directly create more defects as explained in sec. 6.5. The elastic nuclear collisions which are responsible for creating crystal defects occur only toward the end of the ion path. What changes is the depth of the area where the crystal defects are created through the ions.

5.2.2 Variation of the implantation dose

For the purpose of finding out at which boron implantation dose crystal defects begin to occur, the following three implantation doses were implanted:

1. Standard dose: $2.5 \cdot 10^{15}\ cm^{-2}$ (see fig. 27 a)
2. $5.0 \cdot 10^{14}\ cm^{-2}$ (see fig. 27 b)
3. $1.0 \cdot 10^{14}\ cm^{-2}$ (see fig. 27 c)

It was not possible to conduct a NSX analysis of the wafers undergoing these three different implantation doses because there was too large a difference in color between the wafers. As explained in sec. 2.6.5, the core functionality of the NSX inspection system is based on a 'reference wafer' which is used for comparison. Because of the color differences between the wafers, as well as within certain wafers, the NSX method was unable to distinguish between a defect and a difference in the color of the wafer itself.

Therefore, an analysis using a simple optical microscope was performed. The results (see fig. 27 a - c) show a very clear correlation between implantation dose and defect formation. The lower the implantation dose, the fewer defects that occur. This result was expected and is in accordance with the theory about radiation damage (see sec. 6.3)[4].

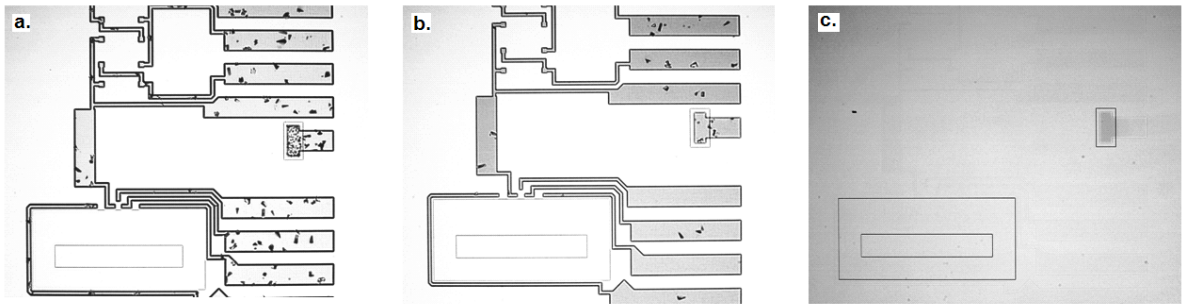

Fig. 27: Defect formation depending on different implantation dose rates. The following dose rates were used: (a) Standard dose: $2.5 \cdot 10^{15}\ cm^{-2}$, (b) $5.0 \cdot 10^{14}\ cm^{-2}$, (c) $1.0 \cdot 10^{14}\ cm^{-2}$. A very clear correlation between the implantation dose and the defect formation was expected and found during this experiment. The standard dose in fig. 27 (a) shows the most defects whereas in fig. 27 (c) almost no defects occur.

5.2.3 Split dose and diffusion time

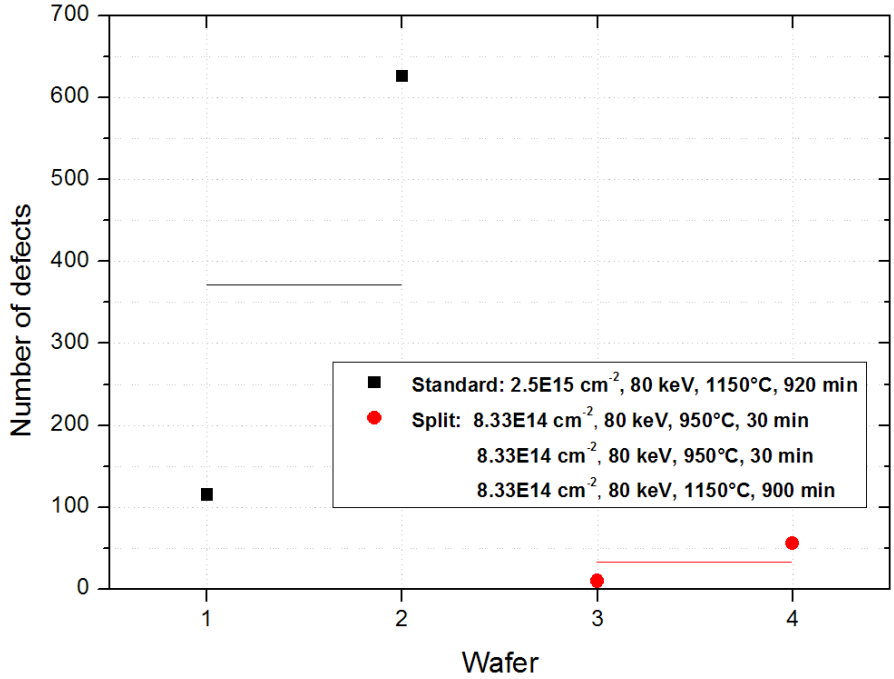

Lot Nr.:	VC815165
X-axis value	Wafer Nr.
1:	10
2:	22
3:	6
4:	20

Fig. 28: Number of defects of wafers undergoing a split in dose and diffusion time.

In this experiment, the dose and diffusion time were split into three steps:

1. $8.33 \cdot 10^{14}\ cm^{-2}$, 80 keV, 950°C, 30 min
2. $8.33 \cdot 10^{14}\ cm^{-2}$, 80 keV, 950°C, 30 min
3. $8.33 \cdot 10^{14}\ cm^{-2}$, 80 keV, 1150°C, 900 min

The results show a clear decrease in defect formation. This could be due to the annealing effect after each diffusion process or to the smaller implantation dose each time. We were able to show a clear correlation between implantation dose and an increase in defects in sec. 5.2.2.

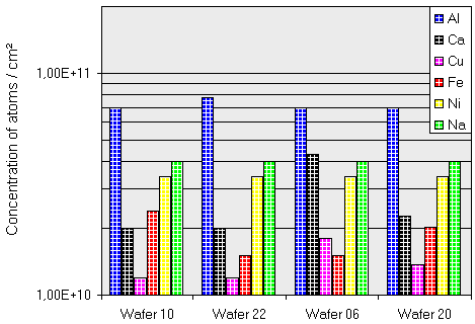

Fig. 29: VPD analysis of wafers undergoing a split in dose and diffusion time.

5.2.4 FZ versus CZ material

The influence of Czochralski-grown versus Float zone-grown silicon upon defect formation was analyzed. The results are shown in fig. 30, with the neighboring table for Infineon references only. As discussed in sec. 2.1, FZ material has a low contamination level regarding carbon, oxygen and metal, whereas the oxygen concentration in CZ material is higher due to chemical reactions between the melted Si and the vessel containing it. The O concentration of the CZ base material used at Infineon Technologies lies between $O = 3 - 6 \cdot 10^{17}\ cm^{-3}$.

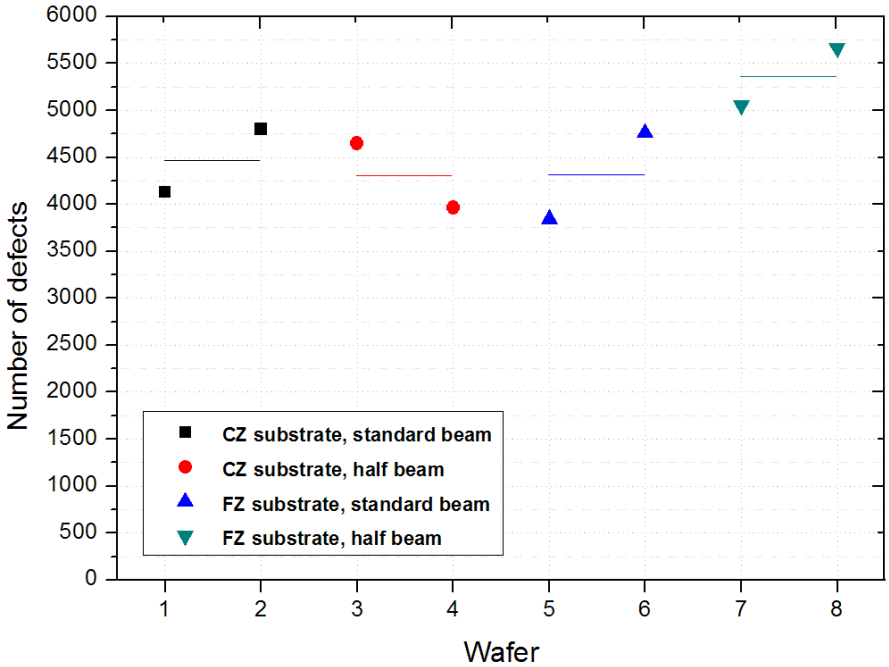

Lot Nr.:	VC820006
X-axis value	**Wafer Nr.**
1:	4
2:	16
3:	2
4:	14
5:	7
6:	10
7:	12
8:	20

Fig. 30: Number of defects in CZ-grown versus FZ-grown material. The number of defects detected by the NSX does not reflect the absolute number of defects on the wafer. It strongly depends on the setting of the NSX setup but enables a comparison of defect formation within the same setup.

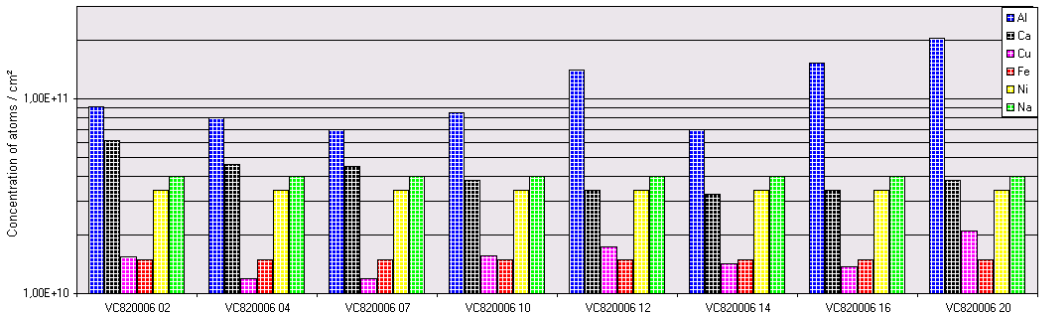

Fig. 31: VPD analysis of CZ grown and FZ grown wafers.

The results of the experiment indicated no distinct change of the defect formation when FZ-grown base material was used. Wafers number 7 and 8 showed a slight increase

of defects, which could have been due to the absence of the gettering function for metallic contaminations of the SiO_2 clusters in CZ material. The VPD analysis of the wafers number 7 and 8 showed higher levels of Al contamination which explained the increase in defects. Wafers numbers 5 and 6 did not show an increase in defects, which could have been due to the lower Al contamination according to the VPD analysis. Wafer number 2 also contained high Al contamination. The SiO_2 clusters of the CZ material might have performed the gettering function, which would explain the lack of defect increase.

5.2.5 Half beam current

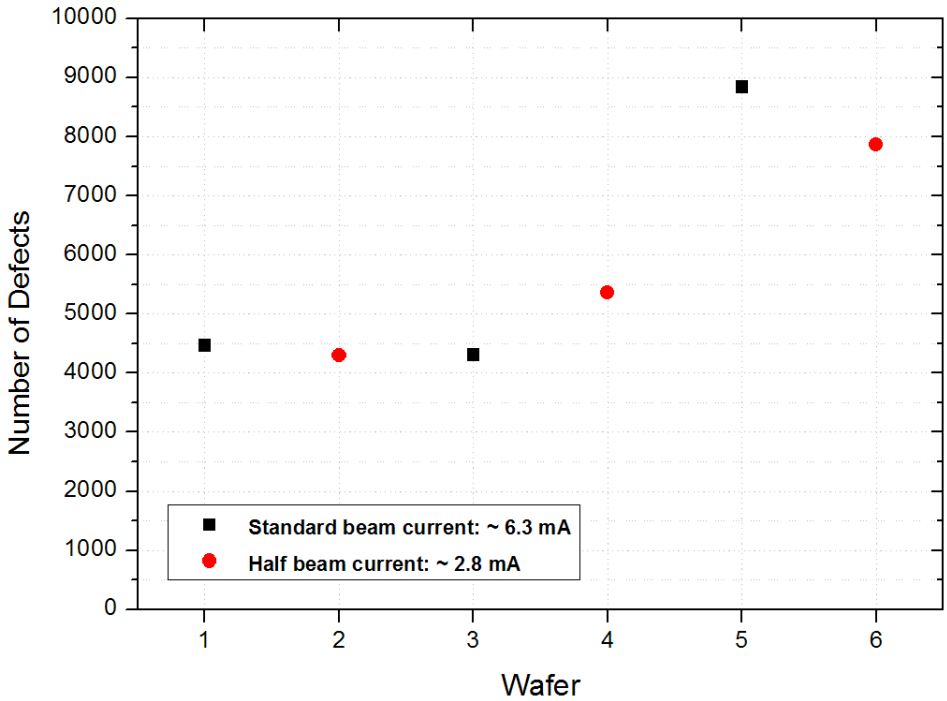

Fig. 32: Change of the defect concentration depending on the beam current. Wafers number 5 and 6 were processed at different times in different lots which generally led to different defect concentrations. The values for the wafers number $1-4$ are the average value of the wafers listed in the table underneath. The increase in defects in wafer number 4 could be related to the higher contamination levels of these wafers. The VPD analyses of the wafers are displayed in sec. 5.2.4 and sec. 5.2.7.

Lot Nr.:	VC820006
X-axis value	**Wafer Nr.**
1:	4 and 16
2:	2 and 14
3:	7 and 10
4:	12 and 20
Lot Nr.:	VC813027
X-axis value	**Wafer Nr.**
5:	4
6:	1

Figure 32 gives a summary of the influence of half a beam current upon defect formation. The implantation time doubles when half the beam current is used because in total the same amount of boron has to be implanted to achieve a specific doping profile after diffusion. In the past, the implantation with half a beam current has led to a decrease in defect formation.

In our experiments, no significant change was found but because of former results which showed an improvement, further experiments using half the beam current will be conducted. The VPD analysis of the wafers in fig. 32 are displayed in sec. 5.2.4 and sec. 5.2.7. The increase in defects in wafer number 4 could be related to the higher contamination levels of these wafers. The higher number of defects in wafers number 5 and 6 occur because these wafers were processed in a different lot than wafers number $1-4$. It is known that the defect concentration varies significantly between different lots containing the wafers. This effect is caused by varying conditions at different times in the production line.

5.2.6 Backside getter layer

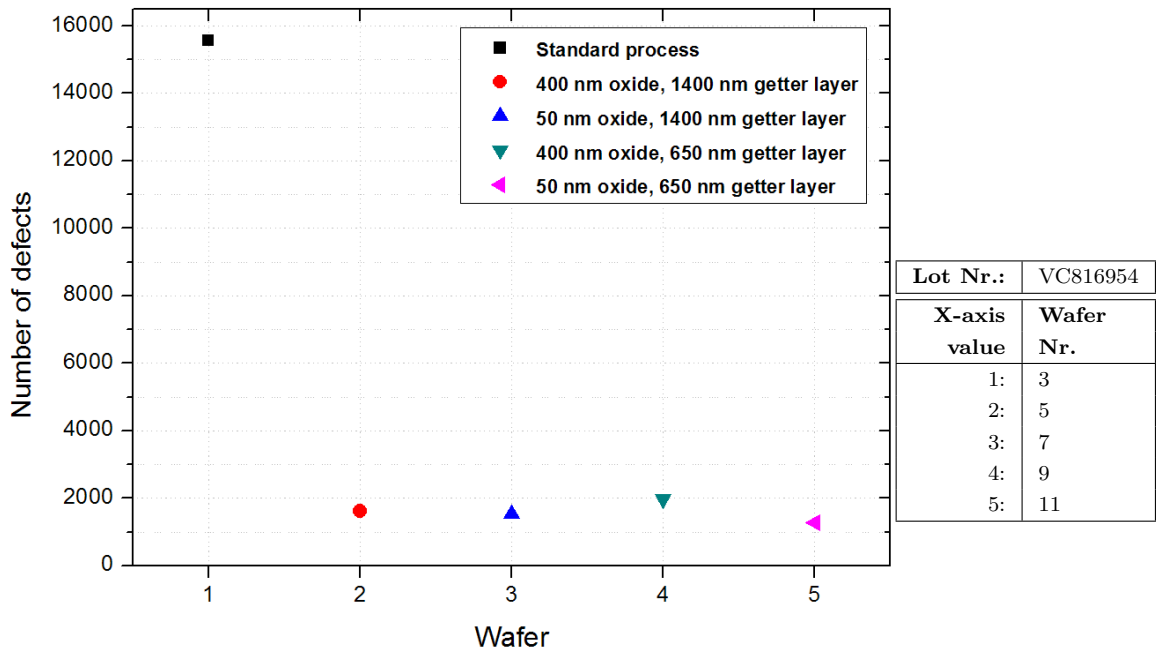

Fig. 33: Number of defects of a wafer with a backside getter layer. The number of defects detected by the NSX does not reflect the absolute number of defects on the wafer. It strongly depends on the setting of the NSX setup but enables a comparison of defect formation within the same setup.

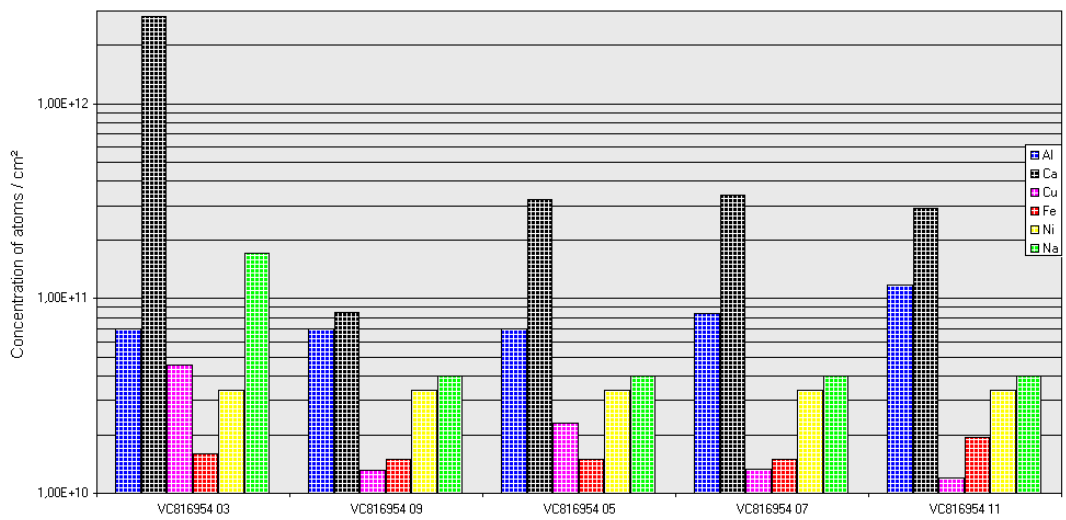

Fig. 34: VPD analysis of wafers with a backside getter layer.

In this experiment, a backside getter layer was added to the wafer. Two different layer thicknesses were chosen, one with 1400 nm and the other with 650 nm. For each thickness a split between a 400 nm oxide and a 50 nm oxide was conducted before adding the getter layer.

The results clearly show a decrease in the number of total defects for all the wafers with a backside getter layer. The VPD analysis of the standard wafer number 1 showed a

high contamination level for Ca which could have also led to a higher number of defects. A difference in the number of defects between the 650 nm and the 1400 nm thick getter layer was not found. Due to the promising results of the backside getter layer and to the problematic contamination level of the reference wafer number 1, further experiments of this kind will be conducted.

5.2.7 Smooth oven processes during phosphorus diffusion

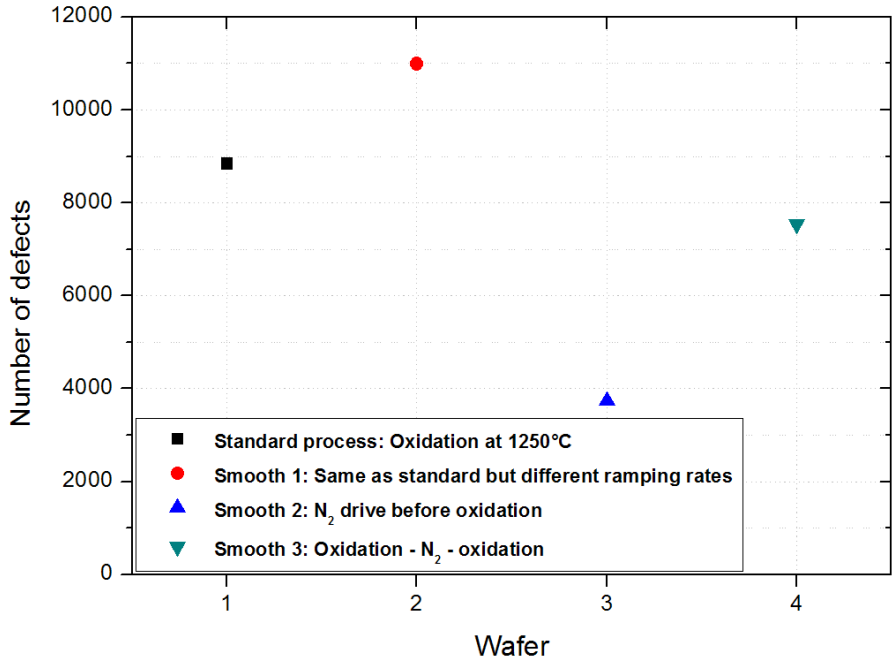

Lot Nr.:	VC813027
X-axis value	Wafer Nr.
1:	4
2:	17
3:	18
4:	19

Fig. 35: Number of defects after smooth oven processes. The number of defects detected by the NSX does not reflect the absolute number of defects on the wafer. It strongly depends on the setting of the NSX setup but enables a comparison of defect formation within the same setup.

Smooth oven processes during phosphorus (membrane) diffusion were developed to minimize the slip lines in the wafer. The goal with this experiment was to create a damage-free silicon surface for the upcoming boron implantation and diffusion. To investigate its influence upon defect formation, one wafer for each one of the three different smooth oven processes was used and compared with a wafer undergoing a standard oven process.

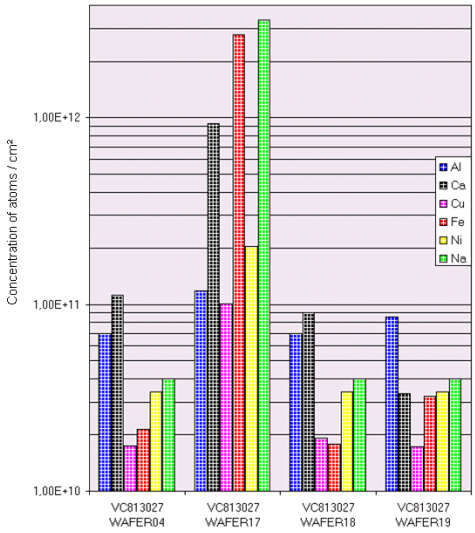

Fig. 36: VPD analysis of wafers undergoing smooth oven processes.

During a standard oven process, the oxidation occurs at $T = 1250°C$, whereas the N_2 drive is carried out after the oxidation. The temperature remains the same in all the smooth oven processes. Smooth 1 is the same as the standard process but uses different ramping rates. During Smooth 2 the N_2 drive is done before the oxidation which, in the past, has led to better results in a reduction of the slip lines. Smooth 3 is a new combination where the oxidation is followed by the N_2 drive which is followed again by the oxidation.

The results showed that the process smooth 2 led to a significant decrease in the number of defects. The defect increase in smooth 1 was probably due to the high contamination

levels as shown in the VPD analysis. Smooth 3 showed no significant change in defect formation.

5.2.8 Base material with higher O_2 concentration

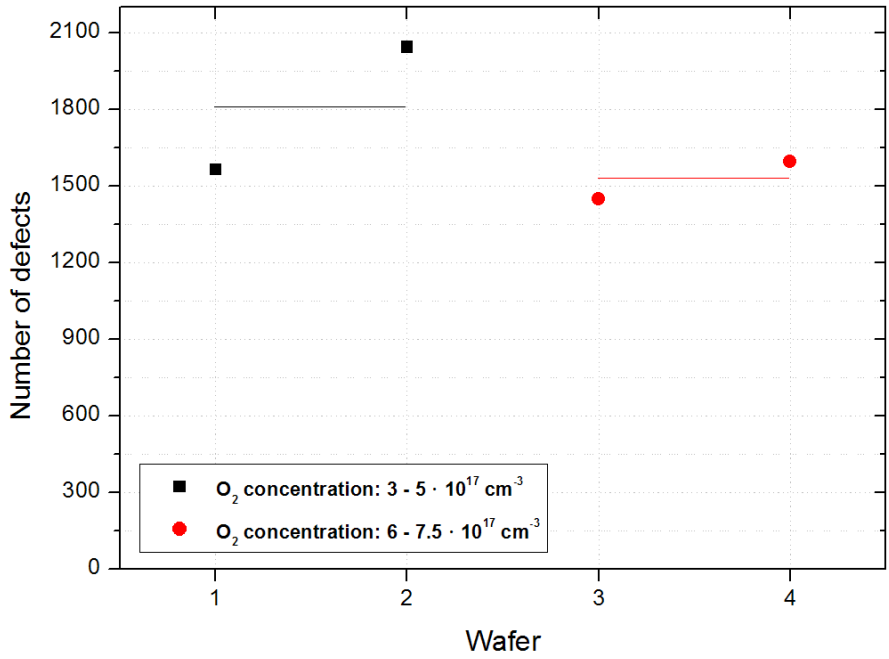

Lot Nr.:	VC819670
X-axis value	**Wafer Nr.**
1:	17
2:	21
3:	5
4:	9

Fig. 37: Number of defects of a base material with a higher O_2 concentration. The number of defects detected by the NSX does not reflect the absolute number of defects on the wafer. It strongly depends on the setting of the NSX setup but enables a comparison of defect formation within the same setup.

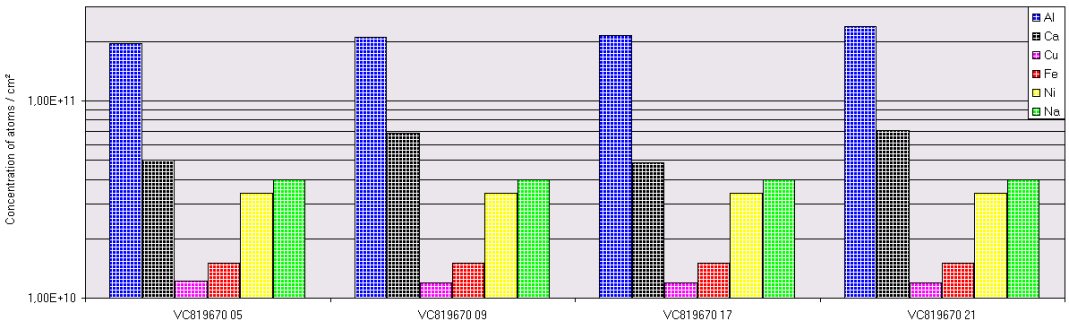

Fig. 38: VPD analysis of a base material containing a high O_2 concentration.

The standard oxygen concentration in the base material was $3 - 5 \cdot 10^{17}\ cm^{-3}$. To investigate the effect upon defect formation with a higher O_2 concentration in the base material, a base material with $O = -7.5 \cdot 10^{17}\ cm^{-3}$ was ordered.

The results found in this experiment were in accordance with the theoretical predictions as discussed in 2.1. On average, a decrease in the number of defects was found in the wafers with the higher O_2 concentration. According to the theoretical background, more oxygen in the base material leads to more microscopic SiO_2 clusters. The associated dislocations perform a gettering function for metallic contaminations and lower critical shearing forces [1].

6 Ion implantation - theoretical background

In ion implantation, atoms or molecules are ionized and accelerated through an electrostatic field. They strike the surface of a wafer and are thereby implanted into it where they constitute ionized impurity atoms in the wafer lattice. The dose of the ion beam can be adjusted and measured, as described in chapter 2.2. The penetration depth of the ion beam depends on the kinetic energy of the ions which can be controlled by adjusting the electrostatic field as well as by the mass of the ions and the atomic mass of the solid. The process is basically not dependent on chemical solubility limits, the temperature of the wafer during implantation, or the concentration of the dopant on the surface of the wafer. The profile of the implanted ions is generally explained with a Gaussian distribution, with an average projected range R_p and a standard deviation ΔR_p. Ion energies range from 10 keV up to several MeV for forming deep structures.
Once ions have been implanted into the wafer, the diffusion process disperses the doped ions from its location, which is close to the surface, more deeply into the wafer and distributes the ions more evenly. Depending on the time and the temperature, different diffusion profiles, which can vary in depth and ion concentration, can be achieved.
For the implanted ions to be electrically active they must come to rest on regular lattice sites after implantation. This is usually not the case for most of the ions, which makes a process called *annealing* necessary. This is a high-temperature treatment which restores the crystal lattice and allows the doped ions to diffuse to electrically-active lattice sites. [4], [5]

6.1 Effects during the bombardment of solids

During the ion bombardment of solids, which stop or scatter ions, there are various effects that take place. Simply they can be listed as [4]:

1. Inelastic collisions with bound electrons of the stopping medium. The energy loss in such collisions takes place by excitation or ionization of atoms or molecules.

2. Inelastic collisions with nuclei. These lead to bremsstrahlung, nuclear excitation or nuclear reactions.

3. Elastic collisions with bound electrons.

4. Elastic collisions with nuclei or whole atoms, whereby a part of the kinetic energy is transferred to the particles absorbing the impact.

5. Cerenkov radiation. This is produced by particles which pass through the medium faster than the phase velocity of light.

Inelastic collisions with electrons, also referred to as electronic stopping, as well as elastic nuclear collisions play the most important role in the stopping of the heavy ions. Depending on the energy and the mass of the accelerated ions, as well as on the atomic number of the medium which is being implanted, one of the two effects will predominate [4].

6.2 LSS theory

LSS theory was the first theoretical analysis of the energy range of ion implantation by Lindhard, Scharff and Schiott (LSS). This theory only considers the interaction of ions with an amorphous medium and therefore does not consider special features like channeling, which is typical for the lattice structure of semiconductors. Therefore, the results of the LSS theory are correct only as a first approximation but are still sufficient to address many practical problems [9]. According to the LSS theory, the range distribution of the ions is a Gaussian one around an average projected range R_p, with a standard deviation ΔR_p (see Fig. 39). When experimental values for the electronic stopping are used for the calculations, the correlation between the LSS theory and measurements of range distribution is especially good. The range distribution in the LSS-theory results from R_p, ΔR_p and the implanted dose D_0:

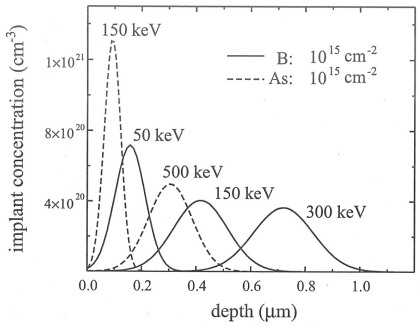

Fig. 39: Theoretical range distribution according to the LSS theory after implantation of boron and arsenic in silicon. [9]

$$N(x) = \frac{D_0}{\sqrt{2\Pi} \cdot \Delta R_p} \cdot exp(-\frac{(x - R_p)^2}{2 \cdot \Delta R_p^2}) \tag{8}$$

The maximum implantation dose N_{max} is described by the prefactor of the exponential function above:

$$N_{max} = \frac{D_0}{\sqrt{2\Pi} \cdot \Delta R_p} \tag{9}$$

The two expressions above are derived under the assumption that the implanted dose D_0 equals the integral over the dose profile $N(x)$ from $-\infty$ to $+\infty$. [2]
The theory does not, however, consider the effects of the stopping process upon the target material, neglects secondary effects like diffusion and only deals with the stopping of the particles [4].

6.3 Radiation damage

Given high enough energy, the mass of the implanted ions atoms can be displaced from their lattice sites and can themselves again displace other atoms. As a result, a **collision cascade** is formed (see fig. 40). As a result of a collision cascade, Frenkel defects as well as complex lattice defects (clusters) occur along the ions path. If the implan-

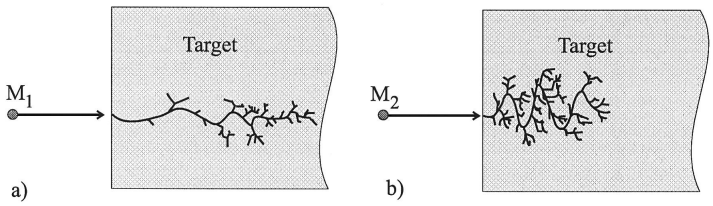

Fig. 40: Schematic representation of the formation of a collision cascade: a) $M_{Ion} < M_{Target}$ as it is the case for a light ion like e.g. boron in silicon; b) $M_{Ion} > M_{Target}$ heavy ion like e.g. arsenic in silicon. [9]

tation dose is increased, the damaged areas begin to overlap and an amorphous layer (see sec: 6.7) extending to a specific depth is created. The amount and distribution of radiation damage depends on the ion species, the temperature, the energy, the dose, and the channeling effects (see sec: 6.6). To measure the amount of radiation damage, one should either consider the number of vacancies produced or the missing energy which has been given off to the solid in the form of nuclear collisions.[4]

6.4 Structure of defects

When a lattice atom is displaced onto an interstitial site, a Frenkel defect is produced and as a result a vacancy and an interstitial atom are left behind [10]. Vacancies can have different charge states, e.g. neutral, positive, negative and double-negative. They can form a complex with impurity atoms and can influence the diffusion of the impurity atoms. If an incident ion displaces two neighboring lattice atoms, double vacancies can be formed. They can also form from two simple vacancies [4]. A group of point defects can reduce its free energy if it agglomerates into a larger defect [5]. Simple defects can also grow during annealing, starting from unannealed radiation damage after implantation and then turning into the undamaged crystal. Furthermore, vacancies or interstitial atoms can accumulate and combinations of impurity atoms with vacancies or interstitial atoms can form further defects.

A local amorphous zone (also known as a cluster) is formed if the implanted ion dose, and thus the concentration of radiation damage, is sufficiently high. Then the damage clusters begin to overlap and an amorphous layer is formed. The critical dose for the formation of an amorphous layer for boron in silicon is $8 \cdot 10^{16}\ cm^{-2}$. [4] Dislocation lines and dislocation loops like the Frank-Read source, which consists of a line of simple

defects with impurity atoms or radiation damage clusters at the ends, can form as a result of stress caused by unannealed radiation damage as well as a combination of simple defects. Along crystal planes, stacking faults can be formed by an accumulation of vacancies or interstitial atoms. These can grow with the addition of further vacancies or interstitial atoms or can be saturated if impurity atoms are added. In this way a gettering effect of the radiation damage can occur. [4]

6.5 Range distribution of radiation damage versus implantation distribution

Because of the fact that the position at which maximum energy is deposited to the target atoms is not the same as the position at which the implanted ions come to rest in the material, radiation damage has a different distribution profile in the solid than the implantation distribution profile of the ions [4]. Ions possessing high energy lose their energy first through electronic stopping. Only toward the end of the ion path do elastic nuclear collisions occur and are responsible for creating crystal defects. The uneven distribution of crystal defects correlates with that observation.
Because of this, the maximum radiation damage is found in a depth where the implanted ions have lost enough energy to finally posses the right amount of energy for elastic nuclear collisions. The maximum radiation damage distribution is always closer to the surface than the maximum ion implantation distribution. [9]

6.6 Channeling effect

As mentioned above, many theories like the LSS theory are based on an amorphous target which by definition means that they have no long-range lattice order. Yet almost all semiconductors are monocrystals and when not then they are at least crystalline. Crystals posses highly anisotropic properties which leads to deviations from theoretical models based on an amorphous medium.
The channeling effect describes the fact that ions can move more deeply into the crystal along its major axes and planes due to the symmetrical arrangement of the lattice atoms in the crystal. Inside these symmetries, which are called channels, are practically no nuclear collisions and the stopping of the implanted ions only happens through electronic stopping. The channeling range is proportional to the kinetic energy of the ions. Silicon possesses a diamond lattice structure with its major axes being: $\langle 110 \rangle$, $\langle 111 \rangle$, $\langle 100 \rangle$. Each major axis possesses a critical angle under which an ion can enter into a channel without leaving it again. At the angles between 7 and 10 the channeling effect is at its minimum. To avoid channeling completely, the target materials surface is made amorphous (e.g. SiO_2) before the ion implantation (see sec: 6.7). The ions are scattered

on the amorphous layer which reduces the number of ions which can penetrate into the channels. [4]

6.7 Amorphous layers

In an amorphous layer the long-range order of the positions of the atoms is non-existent. In microelectronic fabrication an important amorphous form of SiO_2 is called **fused silica**. It is thermodynamically unstable below 1710℃, however the rate of crystallization in the temperature range of interest so slow that it is neglectable. Fused silica does have a short range structure as shown in fig. 41(a). [5]
If the SiO_2 layer is grown in a wet oxidation process, the H_2O present during oxidation will form common water-related complexes which are part of a variety of impurities that can exist in thermal oxides (see fig. 41(b)). The hydrogen atoms are only weakly bonded and can be removed under electrical stress or ionizing radiation. [5]

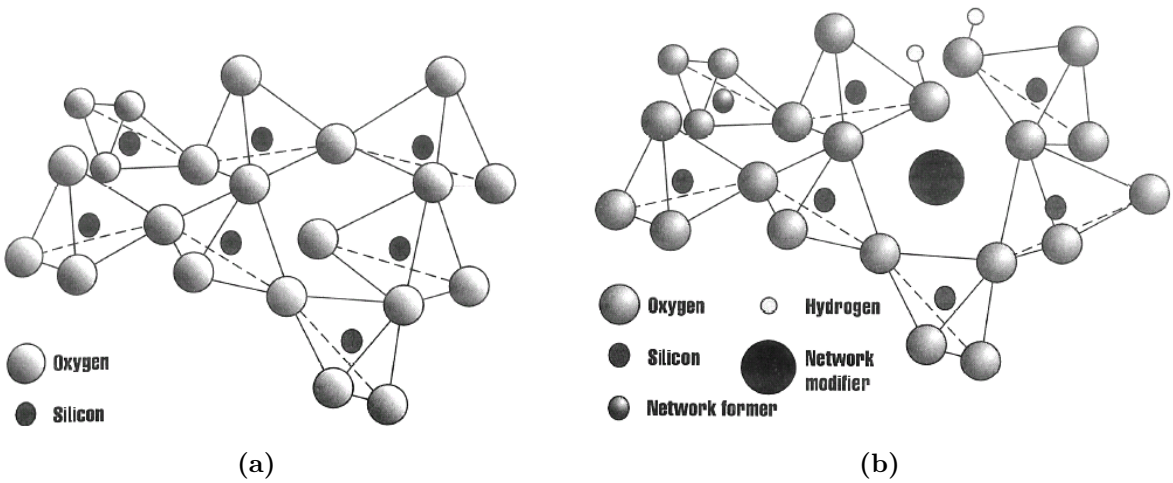

Fig. 41: (a) The physical structure of SiO_2 consists of a silicon atom sitting at the center of an oxygen polyhedra. (b) Schematic description of impurities and imperfections in SiO_2.

7 Summary

In conclusion, from all the experiments which have been conducted during the course of this thesis, the following five processes led to a reduction of the crystal defect formation:

- The deposition of a backside getter layer.
- The N_2 drive before the O_2 oxidation during the phosphorus diffusion (oven process: Smooth 2).
- A split in dose and diffusion time.
- A reduction of the implantation energy.
- Base material with a higher O_2 concentration.

A discussion of the results of the analysis of the deposition of a backside getter layer can be found in sec. 5.2.6. The process smooth 2 and its results are discussed in sec. 5.2.7. The analysis of the split in dose and diffusion time and of the reduction of the implantation energy can be found in sec. 5.2.3 and sec. 5.2.1.
Although the use of a base material with a higher O_2 concentration showed a slight decrease in defects, the practical application is difficult. Because the transition from elastic to plastic deformation occurs only at very high temperatures for a material with higher O_2 concentration, temperature strains lead to dislocations and severe mechanical warping. [5]

Even though the experiments with the half beam current (see sec. 5.2.5) did not result in a clear defect reduction, further investigations into that method will be conducted because in the past a positive improvement has been found.

References

[1] I.Eisele. *Grundlagen der Silizium-Halbleitertechnologie.* 1999. Internal Infineon Material.

[2] M. Glück. *MEMS in der Mikrosystemtechnik.* B. G. Teubner Verlag / GWV Fachverlage GmbH, 2005.

[3] K. Funk R. B. Fair. Ion implantation and junction formation technologies. In *International courses in semiconductor technology.* June 2000.

[4] I. Ruge H. Ryssel. *Ion Implantation.* John Wiley and Sons Ltd, 1986.

[5] S. A. Campbell. *The science and engineering of microelectronic fabrication.* Oxford University Press, Inc., 1996.

[6] H. Foell J. Carstensen, W. Lippik. *Mapping of defect-related silicon properties with the elymat technique in three dimensions.* Report, University of Kiel, Faculty of Engineering, year is unknown.

[7] M. Sperling B. Welz. *Atomabsorptionsspektroskopie.* Wiley-VCH, 4. neubearbeitete Auflage, 1999.

[8] L. Curran. Vision-based semiconductor inspection speeds die processing. *Vision Systems Design*, December 1999.

[9] S. Eichler. *Untersuchungen zu leerstellenartigen Kristalldefekten nach Ionenimplantation in Halbleitern.* Dissertation, Martin-Luther-Universitt Halle-Wittenberg, 1997.

[10] C. Hamann Ch. Weißmantel. *Grundlagen der Festkörperphysik.* Barth, 4. bearbeitete Auflage, 1995.

List of Figures

Danksagung

Diese Arbeit wurde durchgeführt bei Infineon Technologies Austria AG unter der Betreuung von Dr.Techn. Sokratis Sgouridis in Kooperation mit dem Institut für Festkörperphysik unter der Betreuung von O.Univ.-Prof. Dr.Phil. Hartmut Kahlert.

Prof. Kahlert sei herzlich gedankt für die immerwährende Kommunikationsbereitschaft, der kritischen Durchsicht dieser Arbeit und ganz besonders für die freundliche Arbeitsatmosphäre bei den Nachbesprechungen.

Herzlich bedanke ich mich bei Dr. Sokratis Sgouridis und bei Dr. Kai-Alexander Schreiber für die unermüdliche Unterstützung meiner Arbeit bei Infineon. Ihre zahlreichen Anleitungen, Tipps und laufende Bereitschaft mir zu helfen hat den erfolgreichen Abschluss dieser Arbeit erst ermöglicht. Bedanken möchte ich mich an dieser Stelle auch bei Dr. Thomas Neidhart für die Möglichkeit meine Bachelor's Thesis bei Infineon Technologies Austria AG im Zuge eines Praktikums zu schreiben.

Für weitere Hilfestellungen möchte ich mich bei den folgenden Mitarbeitern von Infineon bedanken: Dipl.Ing.(FH) Bernhard Atzberger, Dipl.Ing. Gerd Derflinger, Dipl. Ing.(FH) Hannes Egger, Dr. Robert Koller, Dr. Friedrich Kröner, Dipl.Ing Emil Prax, Josef Riss, Dr. Gudrun Stranzl und Dipl.Ing. Georg Strauss.

Mein Dank gilt auch Dr. Claus Cagran für die zahlreichen LaTeX Tipps und Hinweise, die meine Arbeit sehr erleichtert haben.

An dieser Stelle möchte ich mich auch herzlich bei Mag. Johann Koitz und Mag. Waltraud Koitz für die Aufnahme in Ihrem Heim während meines Aufenthaltes in Villach bedanken. Ihre Herzlichkeit hat alle meine Vorstellungen übertroffen und mir werden die zahlreichen Gespräche und gemütlichen Abende in guter Erinnerung bleiben.

Ein ganz besonderer Dank gilt meinen Eltern und meiner Schwester. Ihr Rückhalt und Ihre Unterstützung über die Jahre hat den erfolgreichen Abschluss dieses Bachelor Studiums erst möglich gemacht.

Zum Abschluss möchte ich mich besonders bei meiner Freundin Monica bedanken, die diese Arbeit so gewissenhaft korrigiert hat. Mit viel Geduld hat Sie die vielen Lernwochenenden miterlebt und hat mir in schwierigen Zeiten immer wieder Mut gemacht und mich motiviert.

Andreas Schriefl